Titre: Title:	Tunable Ferrite Phase Shifters using Substrate Integrated Waveguide Technique
Auteur: Author:	Yon Ju Ban
Date:	2010
Type:	Mémoire ou thèse / Dissertation or Thesis
Référence: Citation:	Ban, Y. J. (2010). Tunable Ferrite Phase Shifters using Substrate Integrated Waveguide Technique [Mémoire de maîtrise, École Polytechnique de Montréal]. PolyPublie. https://publications.polymtl.ca/487/

UNIVERSITÉ DE MONTRÉAL

TUNABLE FERRITE PHASE SHIFTERS USING SUBSTRATE INTEGRATED WAVEGUIDE TECHNIQUE

YONG JU BAN
DÉPARTEMENT DE GÉNIE ÉLECTRIQUE
ÉCOLE POLYTECHNIQUE DE MONTRÉAL

MÉMOIRE PRÉSENTÉ EN VUE DE L'OBTENTION DU DIPLÔME DE
MAÎTRISE ÈS SCIENCES APPLIQUÉES
(GÉNIE ÉLECTRIQUE)
DÉCEMBRE 2010

UNIVERSITÉ DE MONTRÉAL

ÉCOLE POLYTECHNIQUE DE MONTRÉAL

Ce mémoire intitulé:

TUNABLE FERRITE PHASE SHIFTERS USING SUBSTRATE INTEGRATED WAVEGUIDE TECHNIQUE

présenté par : BAN, YONG JU

en vue de l'obtention du diplôme de : Maîtrise ès sciences appliquées

a été dûment accepté par le jury d'examen constitué de :

M. CARDINAL, Christian, Ph. D., président

M. WU, Ke, Ph. D., membre et directeur de recherche

M. DESLANDES, Dominic, Ph. D., membre

DEDICATION

To my lovely wife Jeong Min

And my two sons Jione & Junone

ACKNOWLEDGEMENTS

I would like to express my sincere gratitude to my supervisor, Prof. Ke Wu, for having accepted me and given me the opportunity to pursue my master study in such a challenging and exciting research field, and for his invaluable guidance and encouragement throughout the work involved in this thesis.

I would like to thank Mr. Jules Gauthier, Mr. Jean-Sebastien Décarie and other staffs of Poly-Grames Research Center for their skillful technical supports during my study and experiments. I thank Zhenyu Zhang, Fanfan He and Anthony Ghiotto for their helpful discussions. And many thanks should be extended to Sulav Adhikari for his invaluable supports for my study and thesis.

I also appreciate my colleagues Xiaoma Jiang, Nikolay Volobouev, Adrey Taikov, Marie Chantal, Parmeet Chawala, Jawad Abdulnour and Shyam Gupta in SDP for their understanding and endurance for my study.

Finally my special thanks go to my wife Jeong-Min, my two sons Jione and Junone for their endless love and endurance that encouraged me to the success.

RÉ SUMÉ

Le guide d'ondes intégré au substrat (SIW) est une technique très prometteuse du fait qu'il permet d'utiliser des avantages des guides d'ondes et des lignes de transmission planaires. Comme guide d'ondes, nous pouvons obtenir des avantages tels que de faible pertes, un facteur de qualité élevé, les possibilités de grande puissance et de petit rayonnement. Et comme la ligne de transmission planaire, nous pouvons en faire la fabrication avec une taille compacte et à un faible coût.

Dans ce memoire, des déphaseurs à ferrite sont conçus et expérimentés en utilisant la technique du guide d'ondes intégrée au substrat (SIW) pour profiter des avantages mentionnés ci-dessus. La première tentative de concevoir un déphaseur à ferrite utilisant le SIW a été faite par Wenquan et autres.

Cependant, un résultat expérimental n'a pas été présenté peut-être en raison d'une difficulté de fabrication d'un toroïde de ferrite qui était censé être utilisé dans la conception. Une bonne performance de circulateur de ferrite en structure SIW a été obtenue par William et autres. Cependant, la conception a été implantée dans une polarisation fixe.

Dans cette lettre, des déphaseurs réglables à ferrite utilisant la technique SIW sont présentés et expérimentalement démontrés. Des tores de ferrite sont placés où la polarisation circulaire se produit le long du SIW. La polarisation du champ magnétique statique est appliquée pour magnétiser les tores de ferrite dans la direction transversale.

Dans ce memoire, la méthode de polarisation du champ magnétique variable est présentée et mise en application. Des résultats de mesure et de simulation de phase d'un simple toroïde de ferrite ainsi que celui d'un double toroïde de ferrite seront présentés

Les résultats de mesures des déphaseurs variables à simple et double toroïde de ferrite utilisant la technique SIW ont été présentés. Environ 160° de déphasage a été réalisé avec un déphaseur à simple toroïde de ferrite et 190° de déphasage a été réalisé avec un déphaseur à double toroïde de ferrite. La figure de mérite à 24 GHz avec un déphaseur a double toroïde de ferrite utilisant la technique SIW réalisée dans cette expérience est de 95°/dB.

ABSTRACT

Substrate Integrated Waveguide (SIW) is a very promising technique in that we can make use of the advantages of both waveguides and planar transmission lines. As a waveguide, we can get such advantages as low loss, high Q factor, high power capability and small radiation. And as a planar transmission line, we can fabricate it in a compact size at a low cost. In this letter, ferrite phase shifters are designed and experimented using substrate integrated waveguide (SIW) technique to take advantages mentioned above. The first attempt to design a ferrite phase shifter using SIW was made by Wenquan et al. However, an experimental result was not presented maybe because of a fabrication difficulty of ferrite toroid which was supposed to be used in the design. A quite good performance of ferrite circulator in SIW structure was obtained by William et al. However, the design was implemented in a fixed bias. In this letter, tunable ferrite phase shifters using SIW technique are presented and experimentally demonstrated. Ferrite slabs are placed where circular polarization occurs along the SIW. Static magnetic field bias is applied to magnetize the ferrite slabs in transverse direction. In this letter, a variable magnetic field biasing method is presented and implemented. Measurement and simulation results of both single ferrite slab and double ferrite slabs phase are presented.

Measurement results of a tunable single and double ferrite slab phase shifters using SIW technique were presented. About 160° of differential phase shift was achieved in the single slab ferrite phase shifter and 190° of differential phase shift was achieved in

the double ferrite slab phase shifter. The achieved figure of merit at 24GHz with the double ferrite slab phase shifter using SIW technique in this experiment is 95°/dB.

CONDENSÉ EN FRANÇ AIS

1. Introduction

Le guide d'ondes intégré au substrat (SIW) est une technique très prometteuse du fait qu'il permet d'utiliser des avantages des guides d'ondes et des lignes de transmission planaires. Comme guide d'ondes, nous pouvons obtenir des avantages tels que de faible pertes, un facteur de qualité élevé, les possibilités de grande puissance et de petit rayonnement. Et comme la ligne de transmission planaire, nous pouvons en faire la fabrication avec une taille compacte et à un faible coût.

Dans ce memoire, des déphaseurs à ferrite sont conçus et expérimentés en utilisant la technique du guide d'ondes intégrée au substrat (SIW) pour profiter des avantages mentionnés ci-dessus. La première tentative de concevoir un déphaseur à ferrite utilisant le SIW a été faite par Wenquan et autres.

Cependant, un résultat expérimental n'a pas été présenté peut-être en raison d'une difficulté de fabrication d'un toroïde de ferrite qui était censé être utilisé dans la conception. Une bonne performance de circulateur de ferrite en structure SIW a été obtenue par William et autres. Cependant, la conception a été implantée dans une polarisation fixe.

Dans cette lettre, des déphaseurs réglables à ferrite utilisant la technique SIW sont présentés et expérimentalement démontrés. Des tores de ferrite sont placés où la polarisation circulaire se produit le long du SIW. La polarisation du champ magnétique statique est appliquée pour magnétiser les tores de ferrite dans la direction transversale.

Dans ce memoire, la méthode de polarisation du champ magnétique variable est présentée et mise en application. Des résultats de mesure et de simulation de phase d'un simple toroïde de ferrite ainsi que celui d'un double toroïde de ferrite seront présentés

II. CONSIDÉRATIONS THÉORIQUES ET TOPOLOGIQUES

A. Déphaseur à simple toroïde de ferrite

Un guide d'ondes rectangulaire est synthétisé dans un substrat diélectrique au moyen de deux lignes de via métalliques. Une fente ouverte est usinée dans le SIW de sorte qu'un tore de ferrite soit inséré à la fente ouverte usinée. Puis, chaque ouverture du haut et du bas du mur du SIW est couverte en utilisant une couche mince de cuivre. Afin d'éviter une fuite de micro-onde, les feuilles de cuivre minces sont entièrement soudées au revêtement de cuivre du SIW. La figure 1 montre la géométrie du déphaseur à simple toroïde de ferrite implanté en SIW. Pour les mesures, une transition de SIW au microruban est adoptée. Les détails des paramètres de dimensions utilisés dans la figure 1 sont énumérés dans le tableau 1. Le SIW est fabriqué sur un substrat de RT/duroid 6010.

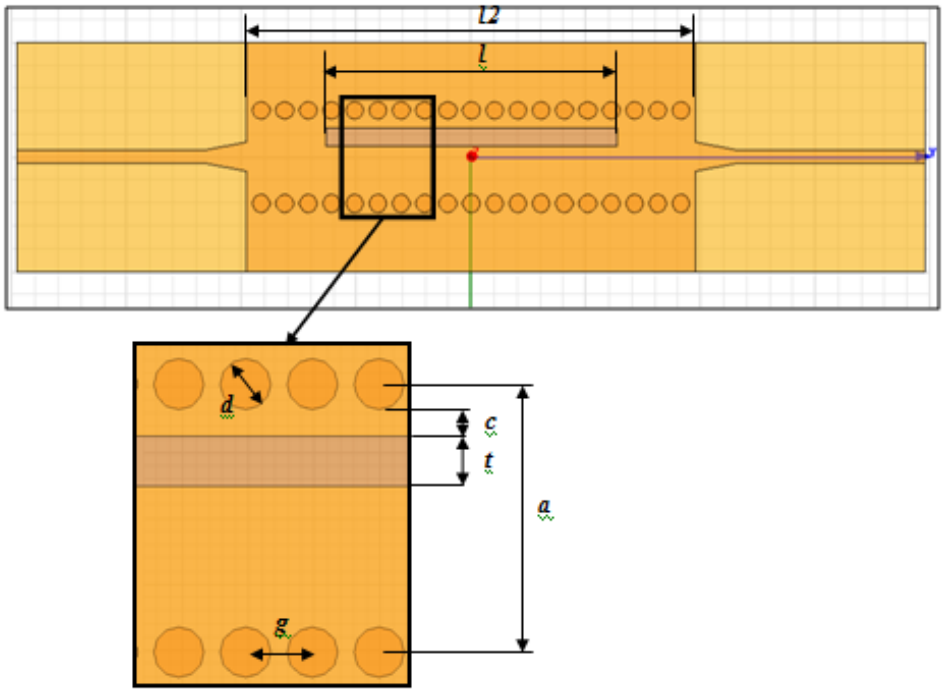

Fig. 1. La géométrie du déphaseur a simple toroïde de ferrite utilisant la technique SIW

Largeur du SIW	*a*	4.064mm
Diamètre des Via	*d*	0.77mm
Distance entre les Via	*g*	1.016mm
Distance de la ferrite au mur	*c*	0.4mm
La longueur du ferrite	*l*	12.7mm
La largeur du ferrite	*t*	0.762mm
La hauteur du ferrite	*h*	0.762mm
La longueur du SIW	*l2*	20mm
La hauteur du substrat	*b*	0.635mm

Table 1. Les paramètres dimensionnels utilisés dans la figure 1

Il y a des régions naturelles de polarisation circulaire dans des guides d'ondes rectangulaires qui fonctionnent en mode TE10. Quand des tores de ferrite sont placés dans ces régions, des ondes de polarisation circulaire sont excitées dans la ferrite parce

que l'onde circulairement polarisée tournant dans la même direction que le dipôle magnétique de précession a une forte interaction avec la ferrite. Le sens de la polarisation (gauche ou droite) dépend de la direction de propagation des ondes dans le guide d'ondes. Les ondes voyageant dans la direction directe dans un guide d'ondes excitent dans la ferrite les ondes de polarisation circulaire avec un sens de polarisation, et les ondes voyageant dans la direction opposée excitent dans la ferrite les ondes de polarisation inverse.

Comme la constante de propagation de l'onde voyageant dans une direction devient différente de celle de l'onde voyageant dans la direction opposée provoquée par une polarisation circulaire différente, il y a des différences de phases liées à la transmission des deux types d'ondes dans le guide d'ondes à ferrite. Quand un tore de ferrite est chargé dans un guide d'ondes, une équation transcendantale pour la constante de propagation β est donnée par

$$\left(\frac{k_f}{\mu_e}\right)^2 + \left(\frac{\kappa\beta}{\mu\mu_e}\right)^2 - k_a \cot k_a c \left(\frac{k_f}{\mu_o\mu_e} cot k_f t - \frac{\kappa\beta}{\mu_o\mu\mu_e}\right) - \left(\frac{k_a}{\mu_o}\right)^2 \times \cot k_a c \cot k_a d$$

$$- k_a \cot k_a d \left(\frac{k_f}{\mu_o\mu_e} cot k_f t + \frac{\kappa\beta}{\mu_o\mu\mu_e}\right) = 0$$

Afin de magnétiser un simple toroïde de ferrite dans un déphaseur SIW, un système de noyau d'électro-aimant est utilisé. Le déphaseur à simple toroïde de ferrite est placé entre deux noyaux d'électro-aimant. Le SIW est fabriqué sur un substrat de RT/duroid 6010 d'épaisseur de 0.762 millimètres et de constante diélectrique de 10.2. Et un tore de ferrite est usiné en TCI NF-5000 qui est une ferrite de nickel. Il a 5000G de saturation magnétique, 100 de "linewidth" et une constante diélectrique de 13

B. Déphaseur a double toroïde de ferrite

Dans la fabrication d'un déphaseur à double toroïde, la seule différence avec celui à simple toroïde est qu'une fente additionnelle est usinée dans le SIW de sorte que deux tores de ferrite puissent être insérés dans le SIW avec une symétrie dimensionnelle entre eux.

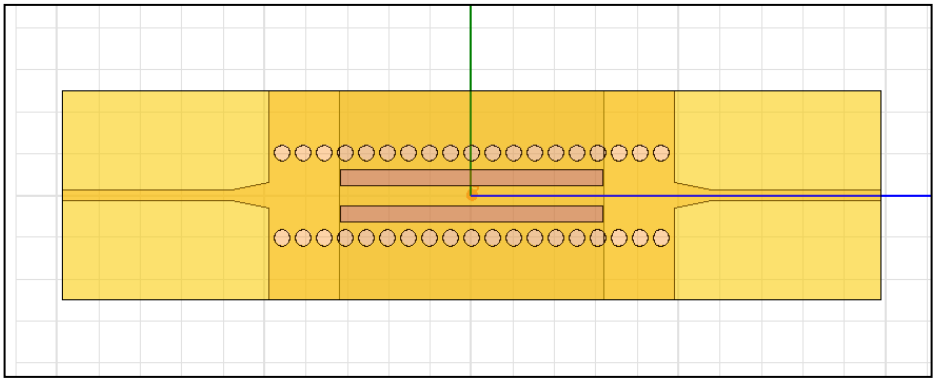

Fig. 2. Vue de dessus du déphaseur à double toroïde de ferrite

L'analyse du déphaseur à double toroïde de ferrite est très semblable à celle de la géométrie à simple toroïde parce que les tores de ferrite des côtés opposés du guide d'ondes sont magnétisés dans la direction opposée, les deux tores de ferrite présentent la même perméabilité à l'onde dans le guide d'ondes et le champ est symétrique. Une équation transcendantale de la constante de propagation, β est donnée par

$$\left(\frac{k_f}{\mu_e}\right)^2 + \left(\frac{\kappa\beta}{\mu\mu_e}\right)^2 - k_a \cot k_a c \left(\frac{k_f}{\mu_o\mu_e} cot k_f t - \frac{\kappa\beta}{\mu_o\mu\mu_e}\right) + \left(\frac{k_a}{\mu_o}\right)^2 \times \cot k_a c \tan k_a d$$

$$- k_a \tan k_a d \left(\frac{k_f}{\mu_o\mu_e} cot k_f t + \frac{\kappa\beta}{\mu_o\mu\mu_e}\right) = 0$$

Pour la magnétisation du déphaseur à ferrite, un système de boucle fermé de champ magnétique est conçu comme montré dans la figure 3 (b). Pour les ouvertures de dessus et de bas du SIW, deux longs plats en acier sont préparés et fabriqués en forme d'Omega. La distance entre les deux extrémités du plat en forme d'Omega a été ajustée pour être identique à celle entre les deux tores de ferrite. Et chaque plat en acier est préparé avec un plaquage en argent de sorte qu'il puisse permettre la soudure. Avant que le plat en forme d'Omega soit soudé à chaque ouverture du SIW, une bobine est enroulée autour du plat de sorte qu'une magnétisation des deux tores de ferrite puisse être réalisée par le courant continu appliqué aux bobines enroulées autour des plats d'Omega.

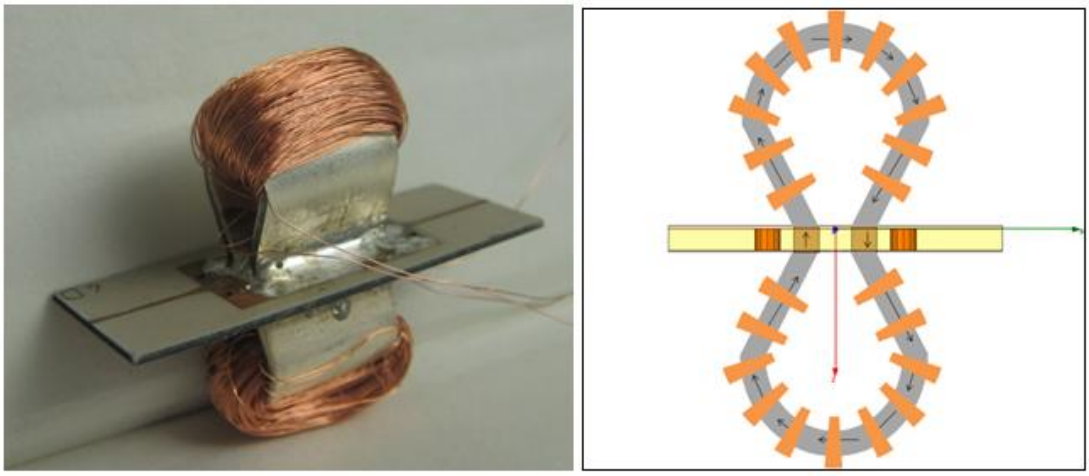

(a) (b)

Fig. 3. (a) Un déphaseur à double toroïde complet utilisant la technique SIW
(b) Une vue en coupe transversale illustrant une boucle fermée de champ magnétique statique

La figure 3 (a) montre un déphaseur à double toroïde complet utilisant la technique SIW technique. Un fil très mince, qui a 0.07mm de diamètre, est enroulé autour de chaque plat en forme d'Omega avec 750 tours.

III. RESULTATS DE SIMULATIONS ET DE MESURES

A. Déphaseur à simple toroïde de ferrite

La figure 3 montre les résultats de mesures et de simulations des pertes de retour d'un déphaseur à simple toroïde de ferrite sans un champ magnétique externe. On constate que plus de 20 dB de pertes de retour peuvent être obtenues en simulation et 15 dB en mesure. La différence entre les résultats de simulation et de mesure peut venir d'une petite ouverture d'air entre les tores de ferrite et la fente ouverte dans le SIW ainsi que d'une armature imparfaite des larges murs faits des bandes de feuilles de cuivre. On constate également que les pertes d'insertion simulées et mesurées sont plus petites que 1.5dB.

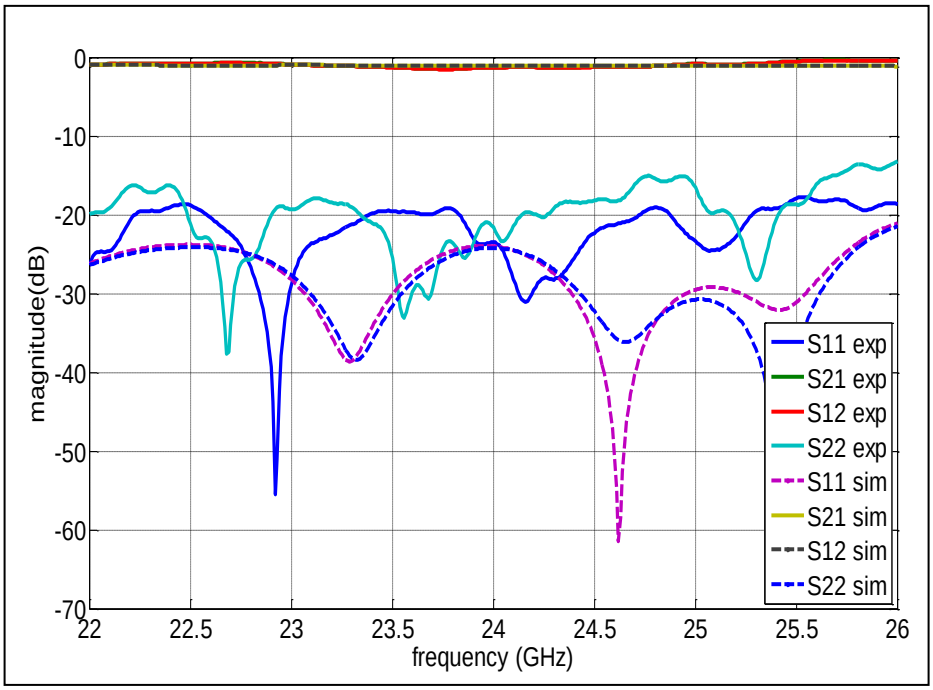

Fig. 4. Les résultats de mesure et simulations d'un depraver SIW à simple toroïde de ferrite sans champs magnétique externe

A partir de la variation de phase entre S21 et S12 par le changement de l'intensité du champ magnétique externe, il est possible de calculer le déphasage résultant du déphaseur à simple toroïde conçu. La figure 5 montre les résultats du déphasage simulé et mesuré. Environ 190° de déphasage a été réalisé en simulation avec 3200G de l'intensité du champ magnétique externe et environ 160° de déphasage est obtenu expérimentalement avec la même intensité du champ. Plus de déphasage pourrait être obtenu si plus d'intensité du champ magnétique externe était appliquée au déphaseur conçu. En regardant la courbe du facteur de démagnétisation, seulement la moitié de la magnétisation a été réalisée dans cette expérience.

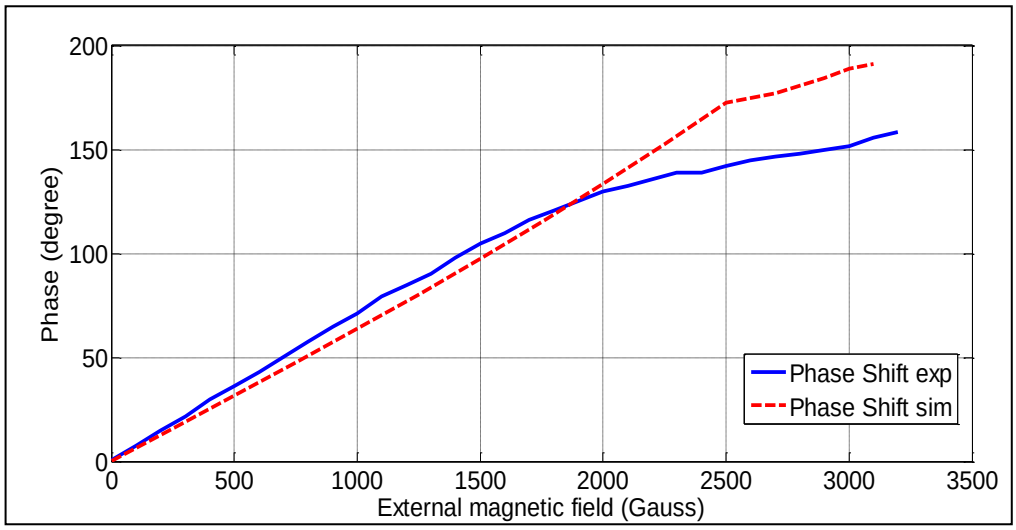

Fig. 5. Résultats de mesure et de simulation du déphasage différentiel à 24GHz

B. Déphaseur à double toroïde de ferrite

Les résultats de simulations et de test des paramètres S du déphaseur à double toroïde de ferrite sont compares dans la figure 6. . Les pertes de retour dans la bande de

fréquences d'intérêt de 22GHz à 26GHz, sont meilleures que 20 dB dans les simulations et 18 dB dans les mesures.

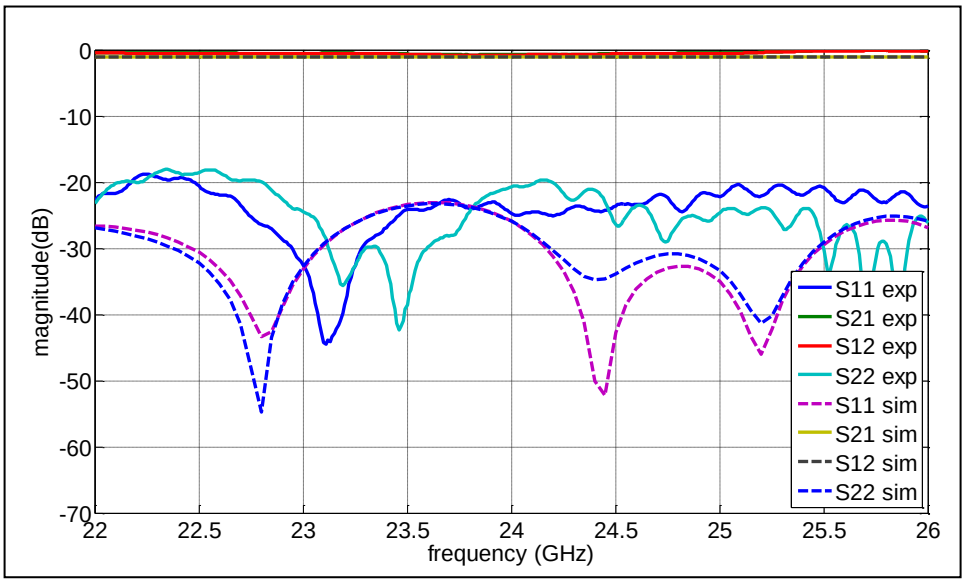

Fig. 6. Résultats de simulation et de mesure du déphaseur à simple toroïde de ferrite sans polarisation du champ magnétique externe

La figure 7 montre le déphasage mesuré du déphaseur à double toroïde. La variation de phase est mesurée en changeant le courant appliqué à la bobine. On peut noter que le déphaseur montre une augmentation linéaire de déphasage en fonction du courant appliqué. Ça signifie que le déphaseur est opéré en-dessous de la saturation magnétique car la perméabilité a une diminution linéaire jusqu'à la saturation magnétique.

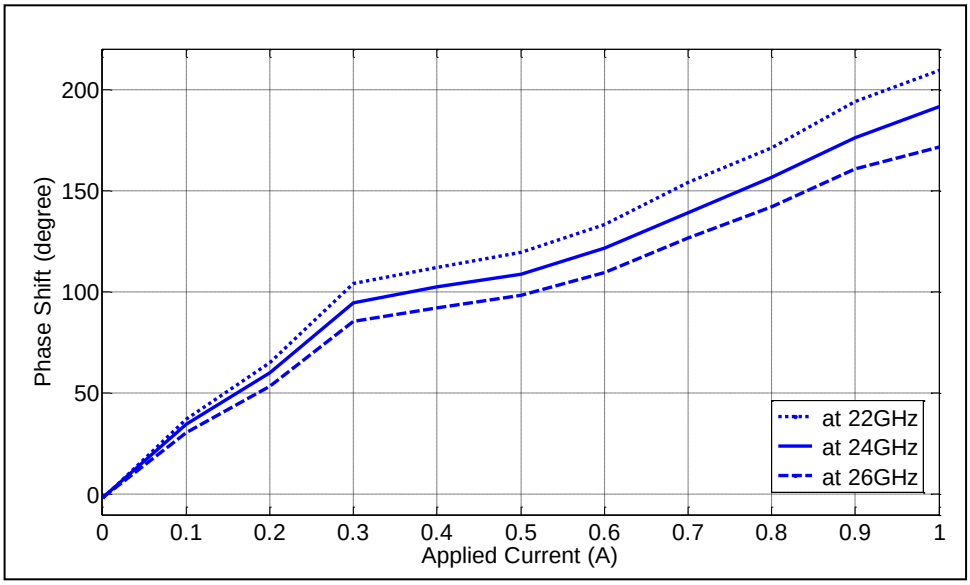

Fig. 7. Résultats de mesures et simulations du déphaseur SIW à simple toroïde de ferrite

Afin de calculer la "Figure de Mérite" du déphaseur à double toroïde de ferrite, les pertes d'insertion ont été capturées par le changement du courant appliqué comme montré dans la figure 8. On observe que les pertes d'insertion de l'onde se propageant dans la direction directe sont déviées de celle de l'onde se propageant dans la direction opposée quand le courant appliqué augmente. Dans cette expérience, la figure de mérite réalisée à 24GHz avec le déphaseur à double toroïde de ferrite utilisant la technique de SIW est de 95°/dB.

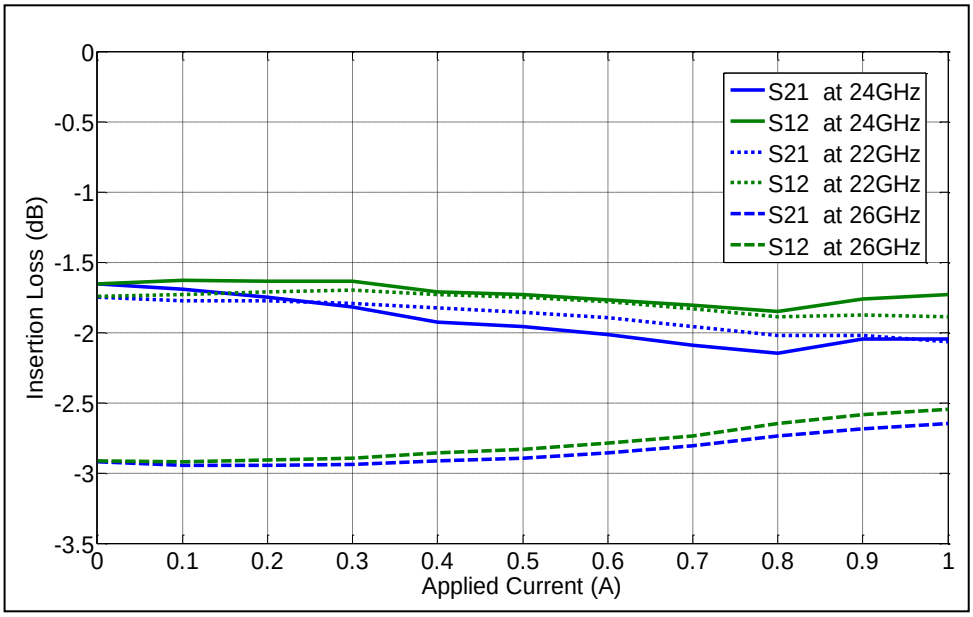

Fig. 8. Les pertes d'insertion mesurées du déphaseur à double toroïde de ferrite

IV. CONCLUSION

Les résultats de mesures des déphaseurs variables à simple et double toroïde de ferrite utilisant la technique SIW ont été présentés. Environ 160° de déphasage a été réalisé avec un déphaseur à simple toroïde de ferrite et 190° de déphasage a été réalisé avec un déphaseur à double toroïde de ferrite. La figure de mérite à 24 GHz avec un déphaseur a double toroïde de ferrite utilisant la technique SIW réalisée dans cette expérience est de 95°/dB.

TABLE OF CONTENTS

TABLE OF FIGURES

TABLE OF TABLES

CHAPTER 1

INTRODUCTION

Substrate Integrated Waveguide (SIW) is a very promising technique with which we can take the advantages of both waveguides and planar transmission lines. With this scheme, we can envision such advantages as low loss, high *Q* factor, high power capability, and small radiation or leakage. And also as a planar transmission line, we can fabricate it with compact size at low cost. Therefore, a large number of vigorous research activities have been seen on SIW technique and various microwave components and devices have been designed successfully using SIW technique. However, there were only few works reported in designing microwave ferrite devices based on SIW technique because there are difficulties in grafting conventional microwave ferrite devices onto SIW structure, which can be described as follows.

a. How to shape and integrate microwave ferrite materials into SIW as ferrites are hard-to-process ceramic materials.
b. How to make a good matching between microwave ferrite materials and laminate materials of SIW.
c. How to design an efficient magnetic field bias system to magnetize the ferrite materials in SIW.

In this thesis, tunable ferrite phase shifters are studied, modeled and experimentally demonstrated using Substrate Integrated Waveguide technique with the consideration of the above-mentioned difficulties.

Microwave ferrite phase shifters are widely used especially for military applications in phased array antenna systems for electrical beam steering by providing different phase states to the radiating elements. The use of nonreciprocal phase shifters in phased array antenna systems is widespread. Ince and Temme, describing both ferrite and diode phase shifters, have studied various antenna feeds and the application of phase shifters [1].

Normally, a typical phased array antenna system consists of a good number of radiating elements, the same quantity of phase shifters are also required. As conventional ferrite phase shifters are made of conventional rectangular waveguide, the manufacturing cost is much higher than its competitive phase shifters and the dimension-related volume is also much larger and heavier. Thus, these drawbacks prevent ferrite phase shifters from being used in commercial applications in spite of their many advantages. Therefore, the development of ferrite phase shifters using planar printed circuit board provides a desirable alternative to the conventional rectangular waveguide ferrite phase shifters.

If a slab of ferrite in waveguide is placed at the position of circular polarization and magnetized perpendicular to the plane of the circular polarization, the effective permeability of the ferrite can be changed by varying the strength of the biasing magnetic field and result in phase shifting of the waveguide. Moreover, since the hand of rotation of the circular polarization is opposite on the opposite side of the waveguide, two ferrite slabs magnetized in opposite directions on opposite sides of the waveguide can yield the most efficient phase shifting [2].

There have been several reported works on the design of ferrite phase shifters based on planar structures. Most of such attempts were implemented utilizing microstrip meander structures. Regarding the research work with the SIW technique, the first attempt to integrate a ferrite toroid into a SIW in order to make a ferrite phase shifter was made by Wenquan Che et al [3]. However, there was no experimental result provided in the paper. Probably it was too difficult to insert a toroidal ferrite core into the SIW as the structure required a quite small size of ferrite toroid.

There was another attempt to design a ferrite phase shifter using the SIW technique and ferrite LTCC materials [4]. However, the measured "figure of merit" in that paper was quite low as compared with other conventional ferrite phase shifters implemented in rectangular waveguides.

There was also a further attempt to integrate a ferrite disk into an SIW circulator was made by William D'Orazio and Ke Wu [5]. It presented a very successful example of circulator design with a simple and clear method of ferrite integration into SIW. However, the magnetic field bias system was not integrated in the design.

The motivation of this thesis work is to study and demonstrate a possibility of designing ferrite phase shifters using SIW technique so that a ferrite phase shifter is fabricated in planar form and manufactured at low cost. If an SIW ferrite phase shifter can be manufactured at low cost with an equivalent "figure of merit" to a conventional rectangular waveguide ferrite phase shifter, the ferrite phase shifter can be very useful for various commercial applications.

This thesis is organized in 5 chapters.

In Chapter 2, basic ferrite theory is reviewed and verified. And it is presented that how the ferrite is chosen and how the ferrite behaves at K band, especially at 25GHz. The definition of Ferrimagnetism is discussed and magnetization equation is introduced. Then, tensor permeability is derived and ferromagnetic resonance is explained. More importantly, based on the basic ferrite theory, it is also described how ferrite materials react when the ferrite is longitudinally magnetized and transversely magnetized, respectively.

In Chapter 3, Substrate Integrate Waveguide (SIW) is presented. First of all, waveguide theory is provided in a brief term and applied to substrate integrated waveguide. Then, design rules of SIW are discussed. A simple SIW is modeled and simulated for K band. Then, a transition from microstrip to SIW is studied and designed.

In Chapter 4, a single ferrite slab phase shifter using SIW technique is designed, fabricated and measured. It is presented that how a ferrite slab is integrated into a simply machined slot in SIW and how an SIW ferrite phase shifter can easily be made. Also, characteristics of finite ferrite materials in practical applications are discussed and applied in the model. To verify the design, nonreciprocal circular polarizations of the single ferrite slab are visualized in 3D model based on HFSS. And then, experimental results are compared with simulation results.

In Chapter 5, a double ferrite slab phase shifter is designed, fabricated and then, measurement results are presented. As a practical design solution of planar ferrite phase shifters, the ferrite phase shifter is devised in a very simple form to be prototyped at low

cost as compared with not only rectangular waveguide devices but also other planar type of ferrite phase shifters. And some design ideas are developed for the ferrite phase shifter in order to reduce the shape demagnetization factor of ferrite slabs such that a more phase shifting can be achieved with lower external magnetic field. At the end of this chapter, the resulting “Figure of Merit” is presented.

CHAPTER 2

MICROWAVE FERRITE THEORY

2.1 Ferrimagnetism

Magnetism is an important part of electrical and electronic circuits and systems. Iron and its alloys are the most abundantly used magnetic materials. However, eddy currents limit the usefulness of iron alloys at high frequencies, whereas ferrites are insulators that are able to provide magnetic cores for high frequency circuits. As magnetic ferrite materials are used in this thesis work, it is necessary to understand the theory behind the magnetic properties of ferrite materials.

Normally microwave ferrite materials can be sorted into three groups, namely spinels, garnets, and hexagonal ferrites.

The ferrimagnetic properties of the spinels ($MOFe_2O_3$) result from the orientation of the net magnetic moments of the metallic ions. The magnetic moments of the ions at the tetrahedral sites cancel the moments of 8 of the ions at octahedral sites. The remaining 8 octahedral ions give the ferrite a net magnetic moment.

Garnets ($3M_2O_35Fe_2O_3$) have crystal structures that are different from those of the spinels in two respects. First, in the garnet structure there are three types of sites for metallic ions, instead of the two site types in the spinel structure. Second, all the sites in the garnet structure are filled.

Hexagonal ferrites ($MO6Fe_2O_3$) have hexagonal crystal structures that make strong magnetic anisotropic energy. The M in the hexagonal ferrites represents Barium, Strontium or some others.

There are two kinds of magnetic moments existing in ferrite materials. The magnetic moment of an ion is the sum of two different moments: one due to the electron spin, and the other due to the orbital motion of the electrons. The magnetic moments of the ions can be calculated from the quantum numbers. Atoms that have only filled shells have no net magnetic moment, because the electron spins and the electron orbital effects cancel each other. The net magnetic moment due to electron spins depends on the number of spins in each direction. If all the spins are up, the moment is equal to the sum of the moments due to each spin. If all the spins are down, the net moment would be determined in the same manner. If some of the spins are up and others down, the difference in the number of spins in each direction would determine the net magnetic moment. [6]

Ferrimagnetism is a hybrid between ferromagnetism and antiferromagnetism as there is an incomplete cancellation of the atomic magnetic moments. Ferromagnetism is the spontaneous alignment of all the atomic magnetic moments, while antiferromagnetism is the complete cancellation of all the magnetic moment in the solid.

One important property of ferrites is that they have very low electric conductivity. For microwave application, the molecules of ferrites are engineered such that ferrites have less mechanisms of conduction.

2.2 Magnetization

The electron behaves as if it were a negatively charged sphere which is spinning about its own axis with a fixed angular momentum. The rotation of charge gives the electron a magnetic moment which is a function of its charge, angular velocity and size. Because of its angular momentum, the electron behaves as if it were a spinning magnetic top whose magnetic moment lies along its axis of rotation. It behaves like a gyroscope, but, instead of moving under the influence of gravitation, it moves due to the influence of magnetic forces which are those of any internal or applied magnetic field. [7]

A magnetic moment in ferrite material may be considered to be a magnetic top, spinning so that the magnetic moment and the angular momentum are parallel vectors. The ratio between the magnetic moment and the angular momentum is a constant for any material and is called the "gyromagnetic ratio" γ. It is given by

$$\gamma = \frac{\boldsymbol{m}}{\boldsymbol{L}} \tag{2.1}$$

where $\boldsymbol{m}$ and $\boldsymbol{L}$ are the magnetic moment and the angular momentum vectors, respectively. Then, the gyromagnetic ratio is given as

$$\gamma = \frac{1}{2} g \mu_0 \frac{e}{m}$$

where g is the Lande spectroscopic splitting factor which is normally close to 2, and e is the charge and m is mass of the electron. We can calculate the gyroscope ratio as $\gamma = 2.21 \times 10^5$ m/C.

In normal case, each magnetic moment is orientated so that there is no torque on it. However, if it is disturbed, the moment will precess as a gyroscope and the torque will be given by the following gyroscope equation [8].

$$\frac{d\boldsymbol{L}}{dt} = \boldsymbol{N} \tag{2.2}$$

As a disturbing magnetic field influences a magnetic moment, the disturbing torque on the moment is the cross-product of the magnetic field and the magnetic moment.

$$\boldsymbol{N} = \boldsymbol{m} \times \left(\boldsymbol{H} + \frac{\boldsymbol{M}}{\mu_0}\right) \tag{2.3}$$

As the individual magnetic moments are all aligned within a domain, it can be assumed that the magnetic moment $\boldsymbol{m}$ is proportional to the magnetization of ferrite material, $\boldsymbol{M}$. Therefore it gives the magnetisation equation as (2.4).

$$\frac{d\boldsymbol{M}}{dt} = \gamma \boldsymbol{M} \times \boldsymbol{H} \tag{2.4}$$

(2.4) is the classical equation of motion of magnetization which is useful because it gives simple mathematical results which are adequate for analysing many low-loss microwave ferrite applications [9].

2.3 Tensor Permeability

When the ferrite material is magnetized to saturation by a static magnetic field, $\boldsymbol{H_0}$ in the z-direction, the magnetic permeability of the ferrite due to an a.c magnetic field becomes anisotropic with rotational symmetry about the direction of the d.c magnetizing field. If the material is magnetized to saturation, it is assumed that all the individual

magnetic moments are aligned within the material. Let there also be a time-varying magnetic field, of time dependence, $\boldsymbol{e^{j\omega t}}$, that is small compared with the saturation magnetic field. [10]

Then the total direction fields in the material will be

Magnetic field intensity: $\boldsymbol{H_0\hat{z} + H}$

which gives rise to

Internal magnetization: $M_0\boldsymbol{\hat{z} + M}$

If substitution of these field values is made into (2.4) and the second order small term $\boldsymbol{M \times H}$ is neglected, we obtain

$$j\omega \boldsymbol{M} = \gamma M_0 \boldsymbol{\hat{z}} \times \boldsymbol{H} - \gamma H_0 \boldsymbol{\hat{z}} \times \boldsymbol{M} \qquad (2.5)$$

Taking the separate components of the field in the rectangular co-ordinate system, (2.5) becomes,

$$\begin{aligned} j\omega M_x &= -\gamma M_0 H_y + \gamma H_0 M_y \\ j\omega M_y &= \gamma M_0 H_x - \gamma H_0 M_x \\ j\omega M_z &= 0 \end{aligned} \qquad (2.6)$$

The first two equations of 2.6 are simultaneous equations in M_x and M_y, therefore (2.6) can be reduced

$$\begin{aligned} M_x &= \chi H_x + j\kappa H_y \\ M_y &= -j\kappa H_x + \chi H_y \\ M_z &= 0 \end{aligned} \qquad (2.7)$$

where

$$\chi = -\frac{\gamma^2 H_0 M_0}{\gamma^2 {H_0}^2 - \omega^2} \tag{2.8}$$

$$\kappa = -\frac{-\omega\gamma^2 M_0}{\gamma^2 {H_0}^2 - \omega^2}$$

The total alternating field is $\boldsymbol{B} = \mu_0 \boldsymbol{H} + \boldsymbol{M}$ and its components are

$$\begin{aligned} B_x &= \mu H_x + j\kappa H_y \\ B_y &= -j\kappa H_x + \mu H_y \\ B_z &= \mu_0 H_z \end{aligned} \tag{2.9}$$

where

$$\mu = \mu_0 + \chi \tag{2.10}$$

The relationship between $\boldsymbol{B}$ and $\boldsymbol{H}$ in (2.8) can be written in vector form

$$\boldsymbol{B} = \mu \boldsymbol{H}$$

where the permeability is the tensor

$$\mu = \begin{vmatrix} \mu & -j\kappa & 0 \\ j\kappa & \mu & 0 \\ 0 & 0 & \mu_0 \end{vmatrix} \tag{2.11}$$

This tensor form of the permeability was first derived by Polder and is often called the Polder tensor permeability [11]. Provided that no reference is made to a specific physical model of the material, μ and κ may be arbitrary quantities which will be constant when the operating frequency and the applied static magnetic field are constant. The relations are generally applicable to any isotropic substance since the only condition needed to be satisfied by the permeability tensor is the rotational symmetry about the axis of the static magnetic field.

If the applied magnetic field is represented by the angular frequency ω_0 and the internal magnetization is represented by ω_m, where

$$\omega_0 = \gamma H_0 \tag{2.12}$$

$$\omega_m = \frac{\gamma M_0}{\mu_0} \tag{2.13}$$

Then μ and κ become

$$\mu = \mu_0 \left(1 + \frac{\omega_0 \omega_m}{\omega_0^2 - \omega^2}\right) \tag{2.14}$$

$$\kappa = -\mu_0 \frac{\omega \omega_m}{\omega_0^2 - \omega^2}$$

ω_0 is the resonant frequency in the ferrite, which is the frequency at which the components of the tensor permeability become infinite and the frequency at which resonance absorption occurs. In a real ferrite material, there are various magnetic loss mechanisms that damp the amplitude attained by the components of the tensor permeability at ferromagnetic resonance.

If a damping term is added to the magnetization equation, the magnetization equation including a damping term is derived as follows.

$$j\omega M = \gamma M_0 z \times H - (\gamma H_0 + j\omega\alpha) z \times M \tag{2.15}$$

where α is a dimensionless damping constant.

It is seen that γH_0 in eqn. 2.5 is replaced by $(\gamma H_0 + j\omega\alpha)$ in eqn. 2.15, and the same substitution may be made in eqn. 2.8 to give the components of the tensor permeability, including losses

$$\chi = -\frac{\gamma M_0(\gamma H_0 + j\omega\alpha)}{(\gamma H_0 + j\omega\alpha)^2 - \omega^2} \quad (2.16)$$

$$\kappa = -\frac{-\omega\gamma M_0}{(\gamma H_0 + j\omega\alpha)^2 - \omega^2} \quad (2.17)$$

with

$\mu = \mu_0 + \chi$

If χ and κ are written as complex quantities to give a field representation of the damping

$\chi = \chi' - j\chi"$

$\kappa = \kappa' - j\kappa"$

The imaginary components of χ and κ give a measure of the power absorbed in the ferrite due to resonance. The resonant linewidth is the width of the resonance which is obtained by varying either the frequency ω or the applied magnetic field H_0, so that the resonance linewidth is specified as $\Delta\omega$ or ΔH.

$$\Delta\omega = \gamma\Delta H = 2\omega_0\alpha \quad (2.18)$$

2.4 Propagation in Longitudinal magnetization

If the wave is propagating in the z-direction with a propagation constant β , and angular frequency ω, following relations between transverse electric fields are obtained,

$(\beta^2 - \omega^2\mu\varepsilon)E_y = j\omega^2\varepsilon\kappa E_x$

$(\beta^2 - \omega^2\mu\varepsilon)E_x = -j\omega^2\varepsilon\kappa E_y$

Eliminating the electric field components gives the propagation conditions of a plane wave

$$\beta^2 = \omega^2 \varepsilon(\mu \pm \kappa) \tag{2.19}$$

There are two solutions for β showing that two modes of propagation are possible which still have all their components of the fields in the transverse plane. The propagation constants are given by,

$$\beta^+ = \omega\sqrt{\varepsilon(\mu - \kappa)} \tag{2.20}$$

$$\beta^- = \omega\sqrt{\varepsilon(\mu + \kappa)} \tag{2.21}$$

There are two possible modes of propagation through a magnetized ferrite material. They have been labelled ‘positive’ and ‘negative’ modes as shown by the notation used in (2.20) and (2.21).

β^+ is the propagation constant of a positive circularly polarized wave and β^- is the propagation constant of a negative circularly polarized wave. It is seen that, for propagation through a magnetically biased ferrite material, circularly polarized modes are the fundamental modes of propagation.

And the constant of proportionality can be shown to be equivalent to an effective free-space impedance of the ferrite material

$$\frac{\beta}{\omega\varepsilon} = \sqrt{\frac{(\mu \pm \kappa)}{\varepsilon}} = \eta^{\pm} \tag{2.22}$$

In the expressions for the phase constant and effective impedance of a circularly polarized wave propagating through a magnetized ferrite material, the same expression

occurs representing an effective permeability of the ferrite medium to the circularly polarized wave. The effective permeability of the ferrite material is defined by

$$\mu^{+} = \mu - \kappa$$
$$\mu^{-} = \mu + \kappa \tag{2.23}$$

The effects of damping in the insulating material may be considered by substituting expressions for the components of the susceptibility tensor into (2.23) as follows.

$$\mu^{+\prime} = \mu_0 + \frac{\gamma M_0(\gamma H_0 - \omega)}{(\gamma H_0 - \omega)^2 - \omega^2\alpha^2} \tag{2.24}$$

$$\mu^{+"} = \frac{\gamma M_0 \omega\alpha}{(\gamma H_0 - \omega)^2 - \omega^2\alpha^2} \tag{2.25}$$

$$\mu^{-\prime} = \mu_0 + \frac{\gamma M_0(\gamma H_0 + \omega)}{(\gamma H_0 + \omega)^2 + \omega^2\alpha^2} \tag{2.26}$$

$$\mu^{-"} = \frac{\gamma M_0 \omega\alpha}{(\gamma H_0 + \omega)^2 + \omega^2\alpha^2} \tag{2.27}$$

The variation of normalized effective permeability with change of static magnetic field at 25GHz is shown in Fig 2.1. In order to plot normalized effective permeability in Fig 2.1, ferrite information of NF-5000 was used from TCI catalogue as shown in Table 2.1. And 25GHz was selected over K band. It is seen from Fig 2.1 that over a specific static magnetic field range, the effective permeability for the positive circularly polarized wave can have a negative value which makes electromagnetic signal unable to propagate through the medium and becomes cut off. Also from the Fig. 2.1, the ferromagnetic resonance is generated when the static magnetic field reaches to about 7.1×10^5 A/m.

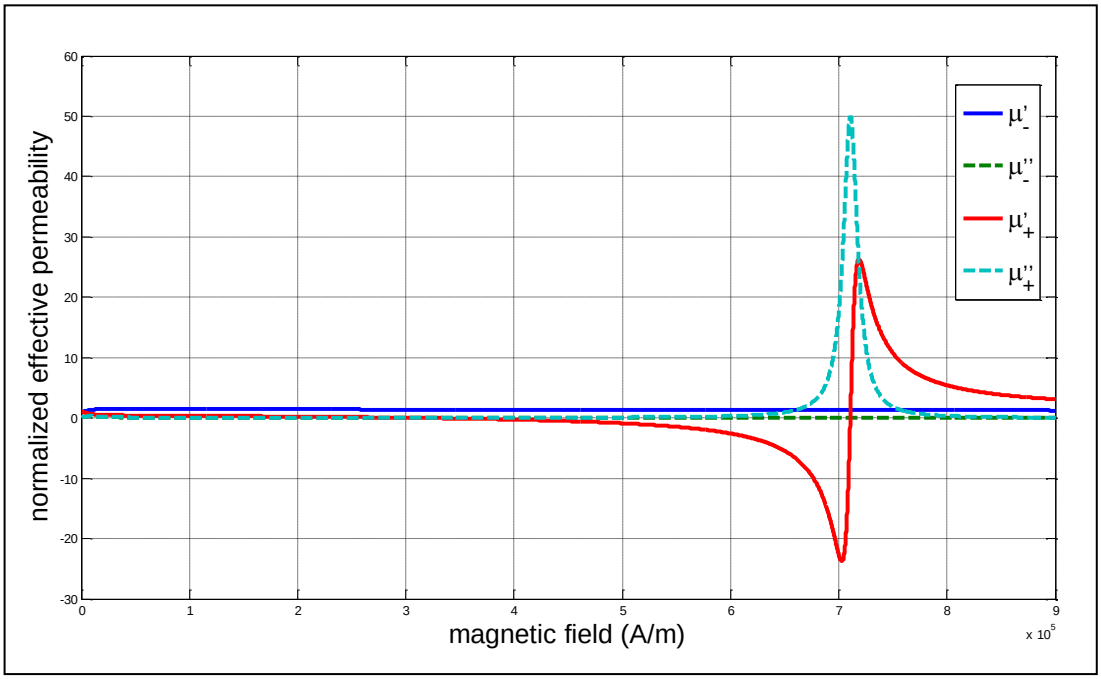

Fig.2.1 Normalized effective permeability with change of magnetic field at 25GHz for the ferrite which has 5000G saturation magnetization.

In order to compare the permeability behavior of various ferrite materials, YG-1780 and LF-4800 were selected from TCI and their permeabilities were compared with that of NF-5000. Therein, YG stands for Yttrium Garnet Ferrite and LF stands for Lithium Ferrite and NF stands for Nickel Ferrite. In general, Yttrium Garnet Ferrite has a low loss characteristic and Nickel Ferrite can be formed with high saturation magnetization. And Lithium Ferrite can retain relatively high residual magnetization for latching ferrite phase shifter applications. In this comparison the specification values of each ferrite material presented in Table 2.1, Table 2.2 and Table 2.3 were used instead of measured values.

Material : NF-5000		
Parameter	Measured Value	Spec.
Dielectric Constant	13.02	13 ±5%
Saturation Magnetization (G)	4799	5000±5%
3dB Linewidth (Oe)	73	≤198
Loss Tangent	0.00046	≤0.0015

Table 2.1 Material Data for NF-5000

Material : LF-4800		
Parameter	Measured Value	Spec.
Dielectric Constant	14.33	14.5 ±5%
Saturation Magnetization (G)	4780	4800±5%
3dB Linewidth (Oe)	189	≤300
Loss Tangent	0.00036	≤0.0010

Table 2.2 Material Data for LF-4800

Material : YG-1780		
Parameter	Measured Value	Spec.
Dielectric Constant	14.83	15.1 ±5%
Saturation Magnetization (G)	1794	1780±5%
3dB Linewidth (Oe)	17	≤17
Loss Tangent	0.0001	≤0.0002

Table 2.3 Material Data for YG-1780

Using the specification data from each ferrite material, the imaginary part of positive permeability of each ferrite material is compared so to describe the ferromagnetic resonance and the linewidth. Fig.2.2 illustrates that YG-1780 makes the narrowest and sharpest resonance trace whereas LF-4800 makes the widest linewidth at the ferromagnetic resonance, and these comply with the material data in Table 2.1 to Table 2.3 in that YG-1780 has the narrowest 3dB linewidth. It is also observed that the resonance of each ferrite material is generated at the same static magnetic field strength as about 7.1×10^5 A/m regardless the magnetization value of each ferrite material.

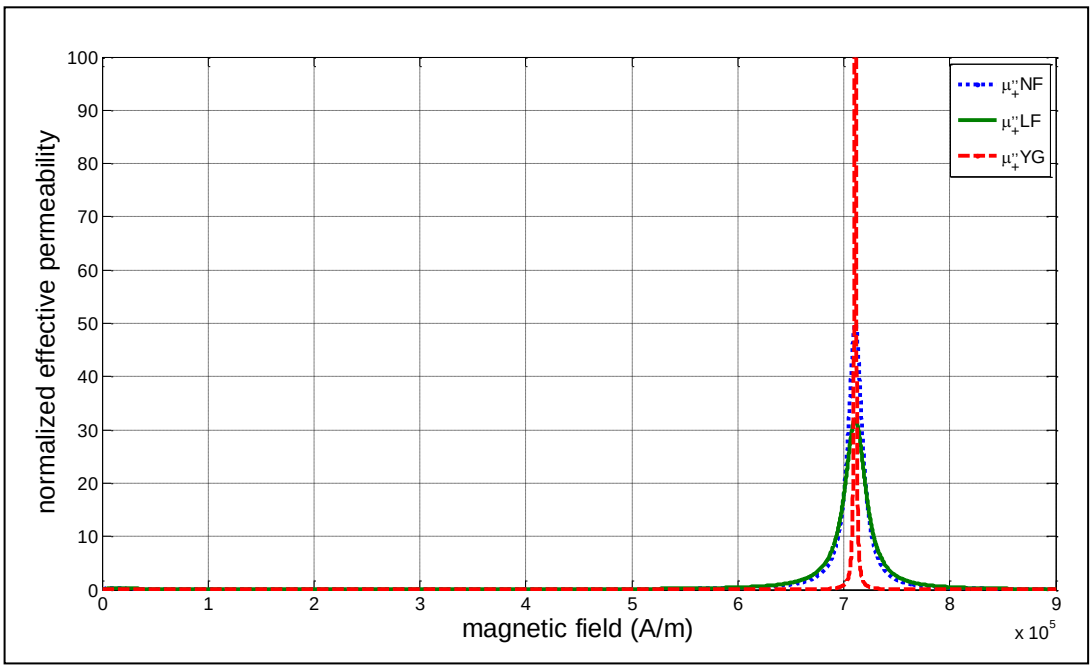

Fig. 2.2 Normalized imaginary part of positive permeability with change of magnetic field at 25GHz for NF-5000, LF-4800 and YG-1780.

In most cases, ferrite phase shifters are operated at a relatively low magnetic field range. Therefore,it is necessary that the effective permeability behavior is carefully investigated by the change of magnetic field until the positive effective permeability of each material reaches to zero value as shown in Fig. 2.3. In order to describe accurately effective permeability at low static magnetic field region, it is also important to understand the permeability behavior in below saturation magnetization region because the most phase shifting can be achieved with below saturation magnetization. However, to our knowledge, there are few papers in the literature that provide a relationship between the permeability of the ferrite material and the applied magnetic field below saturation magnetization. Moreover, ferrite suppliers do not provide permeability

hysteresis traces of their products under a static magnetic field which is necessary to describe effective permeability traces at microwave frequencies.

From the ferrite supplier, it is possible for us to get only an initial permeability value of NF-5000 and YG-1780 as 317 and 134 respectively instead of full permeability traces through B-H tracer. Based on those permeabilities at static magnetic field, the initial permeability of Lithium Ferrite is assumed to be 200 for convenience of calculation. And then the initial permeability values are set under the static magnetic field as constant values until the ferrites are saturated so that we could describe the effective permeability of each ferrite at a given applied magnetic field.

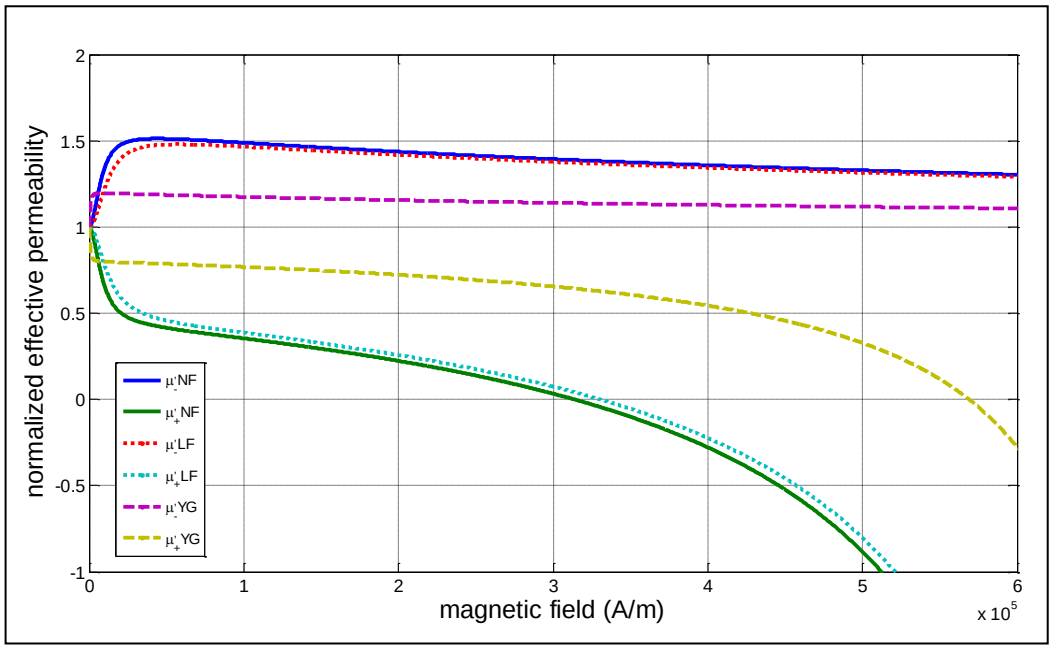

Fig. 2.3 Normalised effective permeability with change of magnetic field at 25GHz for NF-5000, LF-4800 and YG-1780.

According to Fig.2.3, it is observed that a more permeability split can be achieved with Nickel Ferrite (NF) at static magnetic field below 100,000A/m as this ferrite has a higher saturation magnetization than that of Lithium Ferrite (LF) and Yttrium Ferrite (YG).

2.5 Propagation in transverse magnetization

In rectangular waveguides, a common case is that the ferrite is magnetized in a direction perpendicular to the direction of propagation. When the *z*-direction is used as the propagation direction of the plane wave and the *y*-direction is used for the static magnetization, the tensor permeability becomes,

$$\mu = \begin{vmatrix} \mu & 0 & j\kappa \\ 0 & \mu_0 & 0 \\ -j\kappa & 0 & \mu \end{vmatrix} \tag{2.28}$$

Applying the conditions of a plane wave to the two Maxwell curl equations gives

$$\beta^2 H_x = \omega^2 \varepsilon \mu H_x + j\omega^2 \varepsilon \kappa H_z \tag{2.29}$$

$$\beta^2 H_y = \omega^2 \varepsilon \mu_0 H_y \tag{2.30}$$

$$\mu H_z = j\varepsilon \kappa H_x \tag{2.31}$$

These results show that two different modes of propagation are separated, one involving magnetic field component H_y and the other involving magnetic components H_x and H_z although B_z is zero because it is a plane wave. The plane wave described by eqn. 2.30 is a normal linearly polarized plane wave having the propagation constant.

$$\beta^- = \omega\sqrt{\varepsilon\mu_0} \tag{2.32}$$

It is the mode where the magnetic field component is parallel to the direction of the applied static magnetic field. The other mode is also a plane wave described by (2.29) and (2.31). Eliminating the magnetic field components from those equations gives the propagation constant

$$\beta^{+} = \omega\sqrt{\left(\varepsilon\frac{\mu^2-\kappa^2}{\mu}\right)} \tag{2.33}$$

Therefore the effective permeabilities for the linear polarized plane waves in transverse magnetization are

$$\begin{aligned}\mu^{-} &= \mu_0\\ \mu^{+} &= (\mu^2-\kappa^2)/\mu\end{aligned} \tag{2.34}$$

As the + and – no longer apply, parallel and perpendicular as superscripts describe better for directions of linear polarization.

$$\begin{aligned}\mu^{-} &= \mu^{\parallel}\\ \mu^{+} &= \mu^{\perp}\end{aligned} \tag{2.35}$$

Fig.2.4 shows the normalized effective permeability of transverse magnetized NF-5000 ferrite material at 25GHz. As compared with Fig.2.2, it is seen that the static magnetic field required for ferromagnetic resonance is decreased by the factor of the saturation magnetization of the ferrite material used.

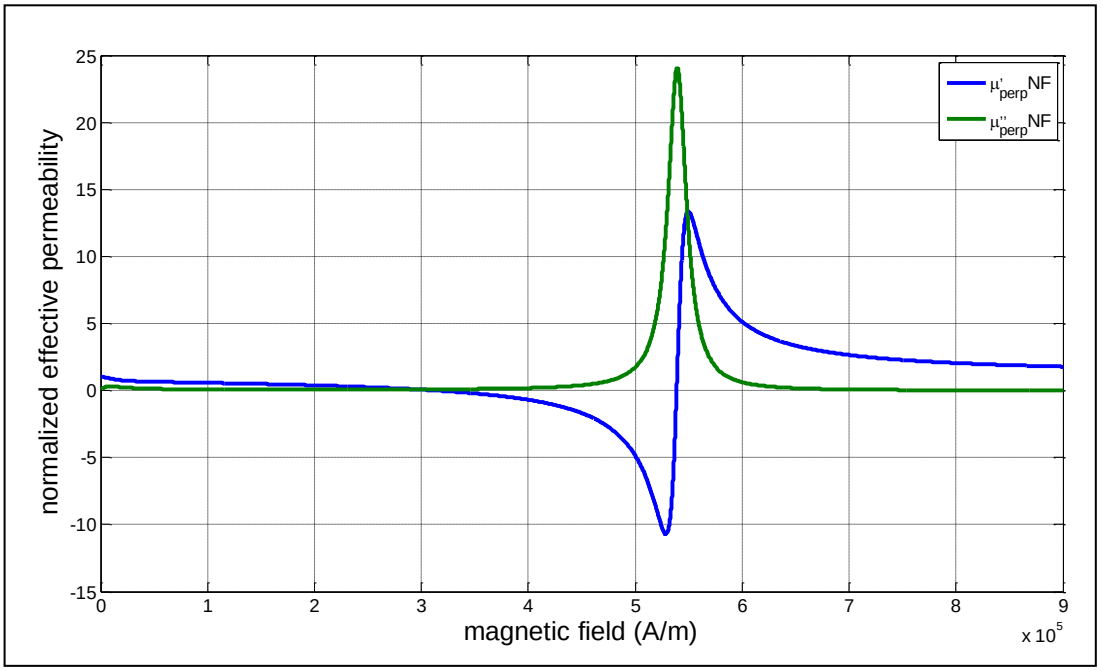

Fig. 2.4 Normalised effective permeability of transverse magnetized NF-5000 with change of magnetic field at 25GHz

In Fig.2.5, the three ferrites, which have different saturation magnetizations and linewidths, are compared together. It is observed that the ferrite material having higher saturation magnetization requires lower static magnetic field to reach ferromagnetic resonance compared with other ferrite materials that have less saturation magnetization. As explained in the longitudinal magnetization case, it is also observed that the Yttrium ferrite (YF) presents the narrowest linewidth.

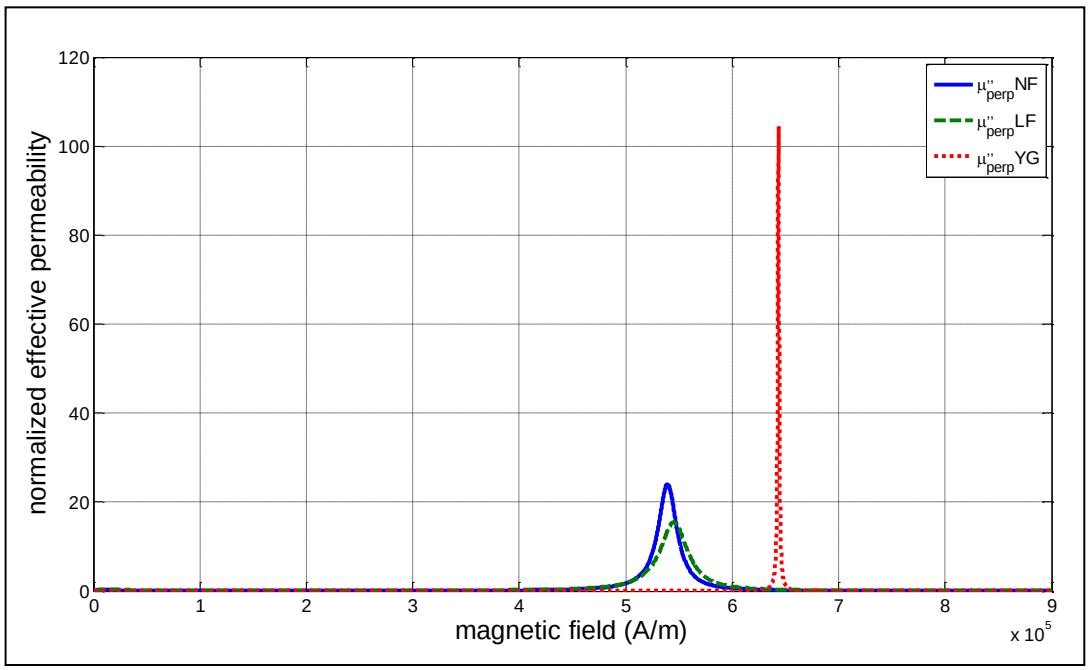

Fig. 2.5 Comparison of normalized effective permeability of transverse magnetized ferrites with change of magnetic field at 25GHz

As the phase shifting in ferrite materials is proportional to the change of the effective permeability, Fig. 2.6 illustrates that a ferrite, which has a higher saturation magnetization, can make more permeability change in perpendicular permeability at low static magnetic field at 25GHz. Therefore, it is also expected that more phase shift can be achieved from ferrite materials that have higher saturation magnetization than that of lower saturation magnetization materials in below saturation magnetization region. However, it should be noted from Fig 2.6 that if the saturation magnetization is increased much high, a specific magnetic field value, which brings the effective

permeability to zero, could be too small such that the phase shift cannot be controlled by the static magnetic field intensity.

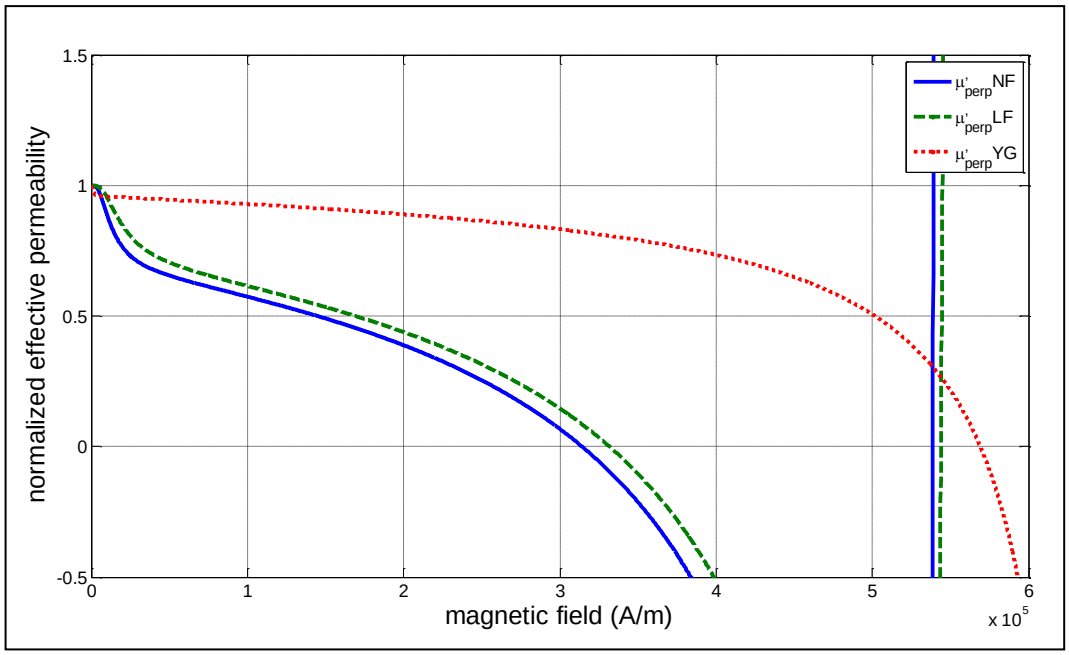

Fig. 2.6 Normalised effective permeability of transverse magnetized ferrites with change of magnetic field at 25GHz

2.6 Conclusion

In this chapter, the microwave ferrite theory was briefly reviewed and tensor permeability was derived. Both longitudinally magnetized ferrite and transversely magnetized ferrite at microwave frequencies were described and explained in term of loss, magnetization and effective permeability. By solving Maxwell equation, we can get

two hands of circular polarized permeabilities. From Fig. 2.3 and Fig. 2.6, it is understood that we can get a more split of circular polarizations at a low static magnetic field if the saturation magnetization value is higher. It is also found that a magnetic field strength of the ferromagnetic resonance of a ferrite is changed by its saturation magnetization value when the ferrite is transversely magnetized whereas that of the ferromagnetic resonance is not affected when the ferrite is longitudinally magnetized.

CHAPTER 3

SUBSTRATE INTEGRATED WAVEGUIDE (SIW)

3.1 Introduction

Waveguide is a traditional transmission line for microwave signal guidance and processing and it is still widely used today for many applications. Various waveguide microwave components such as couplers, detectors, isolators, phase shifters and slotted lines are commercially available for various standard waveguide bands. It is also known that these matured waveguide components present properties of low loss and high power handling. Because of their bulky size, their use is however limited in some of practical applications and it is also difficult to manufacture them in mass production. With trends toward miniaturization and integration, planar transmission line structures such as microstrip and stripline rather than waveguide have been used in many commercial applications. There is, however, still a huge demand for waveguides in loss- and/or power-sensitive applications. Therefore, , it would be much meaningful for microwave applications if we can combine the advantages of planar transmission lines with those of waveguides.

There have been many research activities to develop new platforms of transmission lines to reduce circuit size, simplify manufacture process, lower production cost and maintain high performance. Substrate Integrated Waveguide (SIW) technology is one of

the most popular and the most developed platforms so far as it is quite easy to integrate conventional rectangular waveguide into standard PCB or LTCC [12].

3.2 Rectangular Waveguide

Rectangular waveguide consists of a hollow metal tube of rectangular cross-section which is a closed metal rectangle to transport electromagnetic wave over distances as illustrated in Fig.3.1. The dimensions are a in the x direction and b in the y direction, with the convention that is $a \geq b$ [13]. The boundary conditions are that the tangential component of the electric field must be zero at the four walls of the waveguide:

At $= 0$: $E_y = 0$ and $E_z = 0$

At $x = a$: $E_y = 0$ and $E_z = 0$

At $y = 0$: $E_x = 0$ and $E_z = 0$

At $x = b$: $E_x = 0$ and $E_z = 0$

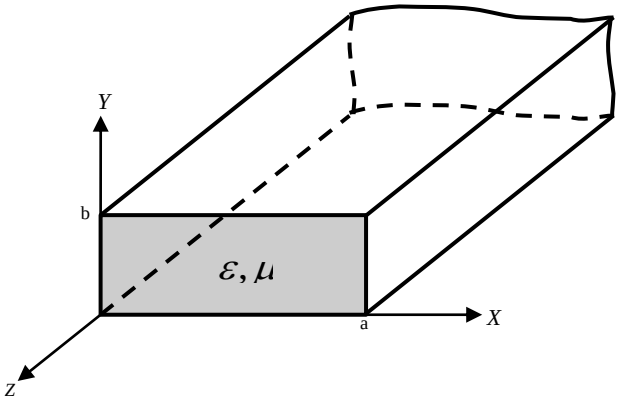

Fig.3.1 Geometry of a Rectangular Waveguide

Due to the single connected conductor geometry, rectangular waveguide does not support the propagation of TEM mode. TE and TM are the modes of propagation in a rectangular waveguide. While, in an SIW only the propagation of TE modes is possible.

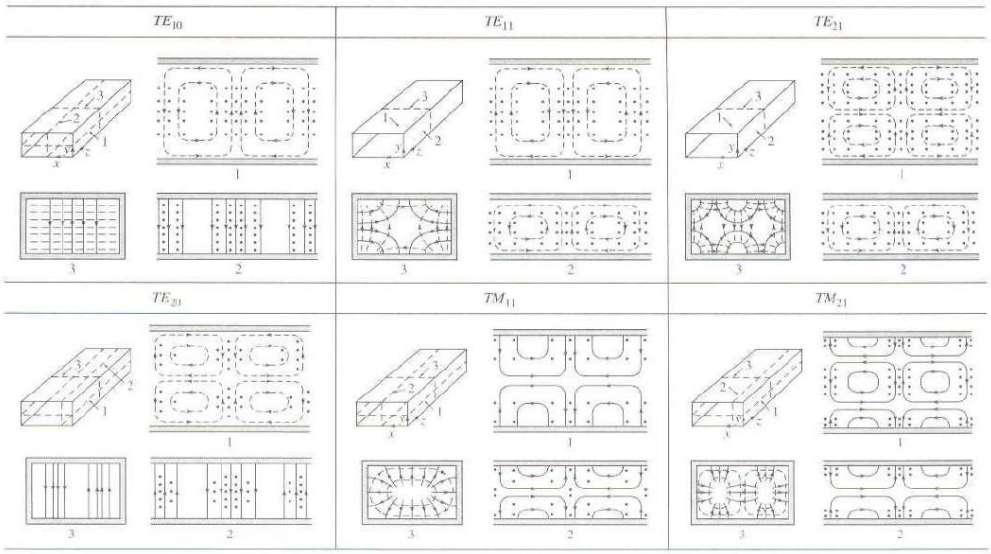

Fig.3.2 Various modes in rectangular waveguide [14]

3.3 Wave Propagation in Waveguide

The geometry of an arbitrary waveguide is shown in Fig. 3.1. This structure is assumed to be uniform in the z direction and infinitely long.

The transverse field components of the TE_{mn} modes can be found by assuming $E_z = 0$. Once $H_z = A_{mn} cos \frac{m\pi x}{a} cos \frac{n\pi y}{b} e^{-j\beta_{mn} z}$ has been found, the transverse components are given by

$$
\begin{aligned}
E_x &= \frac{j\omega\mu n\pi}{k_c^2 b} A_{mn} \cos\frac{m\pi x}{a} \sin\frac{n\pi y}{b} e^{-j\beta z} \\
E_y &= \frac{-j\omega\mu n\pi}{k_c^2 a} A_{mn} \sin\frac{m\pi x}{a} \cos\frac{n\pi y}{b} e^{-j\beta z} \\
H_x &= \frac{j\beta m\pi}{k_c^2 a} A_{mn} \sin\frac{m\pi x}{a} \cos\frac{n\pi y}{b} e^{-j\beta z} \\
H_y &= \frac{j\beta n\pi}{k_c^2 b} A_{mn} \cos\frac{m\pi x}{a} \sin\frac{n\pi y}{b} e^{-j\beta z}
\end{aligned}
\tag{3.1}
$$

where integer *m* and *n* describe the numbers of variation of the fields along the two transverse coordinates.

$$
k_c^2 = k_x^2 + k_y^2 = \left(\frac{m\pi}{a}\right)^2 + \left(\frac{n\pi}{b}\right)^2 \tag{3.2}
$$

When $\beta = 0$, The TE modes cannot propagate along the Z axis or the modes are cutoff.

$$
k = k_c = \sqrt{\left(\frac{m\pi}{a}\right)^2 + \left(\frac{n\pi}{b}\right)^2} \tag{3.3}
$$

Then

$$k = \omega\sqrt{\mu\varepsilon} = \sqrt{\left(\frac{m\pi}{a}\right)^2 + \left(\frac{n\pi}{b}\right)^2} \tag{3.4}$$

Equation (3.9) implies that each TE mode has associated with a characteristic cutoff frequency $f_{c.m.n}$, below which the mode does not propagate. Therefore, the cutoff frequency of each mode is

$$f_{c.m.n} = \frac{k_c}{2\pi\sqrt{\mu\varepsilon}} = \frac{1}{2\pi\sqrt{\mu\varepsilon}}\sqrt{\left(\frac{\pi m}{a}\right)^2 + \left(\frac{\pi n}{b}\right)^2} \tag{3.5}$$

The cutoff frequency $f_{c.m.n}$ is a geometrical parameter dependent on the waveguide cross section dimensions.

3.4 Substrate Integrated Waveguide

Rectangular waveguide is known for its feature properties of low loss and high power handling. However, its bulky structure makes it difficult to fabricate it at low cost and integrate it into planar structure. Table 3-1 shows the comparison of characteristics for several transmission lines [15].

Table 3-1. Comparison of Characteristic for several transmission lines

Transmission Line	Frequency Range (GHz)	Q-factor	Power Handling	Integration with other components	Potential for low cost production
Rectangular Waveguide	<300	High	High	Poor	Poor
Coaxial Line	<50	Moderate	Moderate	Poor	Poor
Microstrip line	<100	Low	Low	Good	Good
Slot-line	<60	Low	Low	Good	Good
Coplanar Waveguide	<100	Low	Low	Good	Good

Typical integrations from rectangular waveguide to planar structure are bulky and usually require a precise matching process. Furthermore, the planar substrate has to be cut into a specific shape for matching. These constraints make the integration difficult and costly.

A straightforward solution is to integrate the rectangular waveguide into the microstrip substrate. The will surely reduce the Q factor of the waveguide because of dielectric filling and volume reduction. However, the entire circuit including planar circuit, transition and waveguide can be constructed using standard PCB or other planar processing techniques [16].

In general, Substrate Integrated Waveguide (SIW) is the synthesized rectangular waveguide built in the standard PCB or dielectric substrate by placing two discrete metallic via-hole arrays [17] .

A typical geometry is shown in Fig. 3.3 where metallic via-hole arrays work as side walls of the waveguide while the substrate's metal cover and ground plane form the

waveguide broad walls. From microwave point of view, the wave propagation is well confined between two arrays of the metallic via holes which can be considered as non-radiating electric walls from the microwave point of view. Each gap between two via holes can be viewed as a holder to support and prevent the waveguide from falling down from the substrate. An appreciative gap size is critical to minimize lateral radiation loss or wave leakage [18].

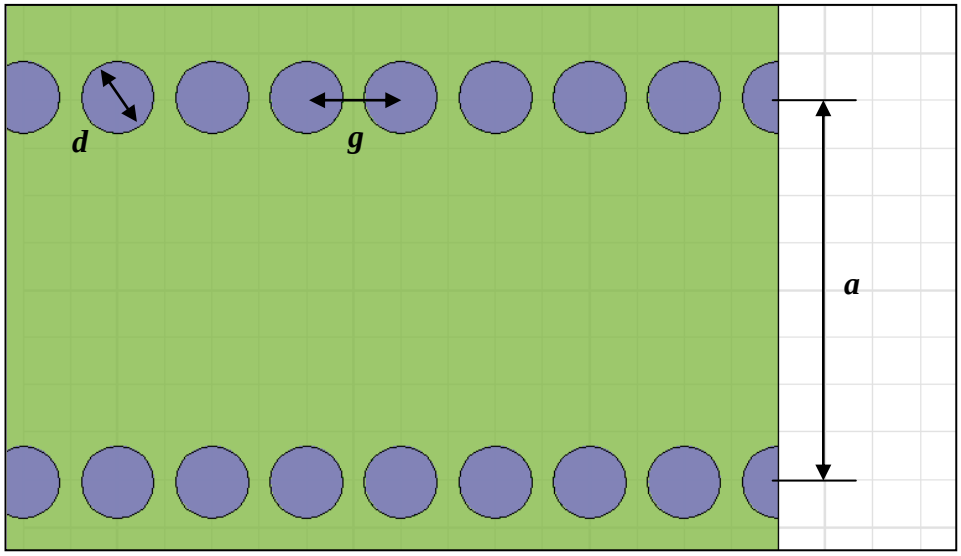

Fig. 3.3 Configuration of the SIW synthesized by metallic via-hole arrays

3.5 Characterization of Substrate Integrated Waveguide

As mentioned earlier, SIW is composed of two parallel arrays of via holes delimiting the TE_{10} wave propagation area, as its cutoff frequency is only related to the width *a* of the waveguide as long as the substrate thickness or waveguide height *b* is smaller than *a*.

Parameter *a* between the two arrays determines the propagation constant of the fundamental mode, and parameters of via holes *d* and *g* are set to minimize the radiation loss as well as the return loss.

Though SIW can be characterized by propagation constant, waveguide mode, cutoff frequency and guided wavelength like a conventional rectangular waveguide, it should be noted that SIW has some peculiar physical characteristics as compared with conventional rectangular waveguides.

First, the SIW's geometrical parameter *a* is much larger than *b* because there is a physical limitation to increase the substrate thickness *b*. Second, the equivalent waveguide width of SIW, a_{eff} is not the same as *a*. Therefore, many experiments and simulations have been conducted to verify value of a_{eff}. One empirical equation to calculate a_{eff} is given by (3.6) [18].

$$a_{eff} = a - 1.08\frac{d^2}{g} + 0.1\frac{d^2}{a} \tag{3.6}$$

when $d/g < 1/3$ and $d/a < 1/5$.

SIW can be modeled by rectangular waveguide with an equivalent width and maintains radiation loss at a negligible level, when its geometry parameters meet

$$\begin{aligned} d &< \lambda_g/5 \\ g/d &\le 2 \end{aligned} \tag{3.7}$$

where λ_g is the guide wavelength related to a_{eff}.

In order to make an SIW working for K-band applications in this thesis, the cutoff frequency of TE_{10} mode in SIW is selected about 13.5GHz with the following considerations.

a. TE_{20} mode should not be excited in SIW.
b. The physical width should be as wide as possible so that ferrite slabs can be inserted.

Figure 3.4 shows the simulation results of SIW designed with the following parameters on Rogers RT/Duroid 6010 with dielectric constant of 10.2. Normally, the dielectric constant of a ferrite material is around 13 ~ 15 and the highest dielectric constant of commercial high frequency laminate materials we can get is 10.2. Therefore, This laminate material can minimize the expected mismatching problem between the dielectric laminate material and the ferrite. In order to avoid any difficulty in inserting ferrite slabs into the SIW, a relatively thick laminate material was chosen so as to make the machining of ferrite materials easier.

Table 3.1 Parameters for Substrate Integrated Waveguide used in Fig 3.3

Width	a	4.064mm
Effective width	a_{eff}	3.448mm
Via hole diameter	d	0.77mm
Gap between vias	g	1.016mm
Substrate thickness	b	0.635mm

Table 3.1 shows the calculated parameters based on (3.5), (3.6) and (3.7) with the consideration of SIW machining and ferrite slabs. From the calculated effective width of

broad wall, the cutoff frequency of TE_{10} mode in SIW is about 13.5GHz. This frequency is the optimal frequency that can satisfy both of the above considerations.

Using the parameters in Table 3.1, Fig. 3.4 shows a simulated result of the SIW in Fig 3.3. The simulation result agrees well with the calculated cutoff frequency of 13.5GHz.

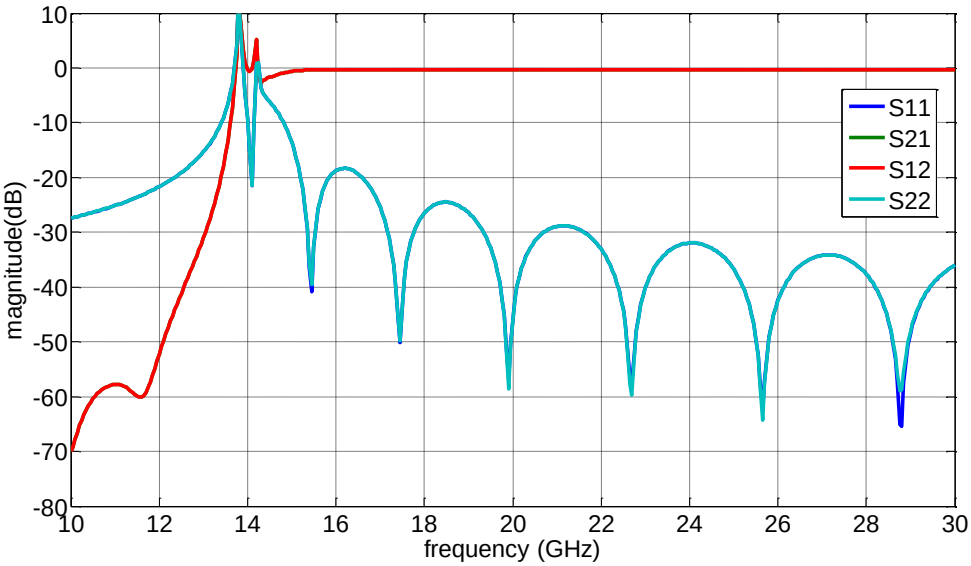

Fig. 3.4 Simulation results of the K band SIW

3.6 Transition from Microstrip to SIW

In order to make a good transition from the microstrip to the SIW, first of all, it is necessary to calculate the guide impedance of the SIW which is given by (3.8)

$$\boldsymbol{Z_{pi} = Z_{TE}\frac{\pi^2 b}{8a}} \tag{3.8}$$

For the calculation of the guide impedance, it is also necessary to calculate the wave impedance of TE mode which is given by

$$\boldsymbol{Z_{TE}} = \frac{\boldsymbol{j\omega\mu}}{\boldsymbol{\gamma}} = \frac{\boldsymbol{\omega\mu'}}{\boldsymbol{\beta}} = \sqrt{\frac{\boldsymbol{\mu}}{\boldsymbol{\varepsilon}}} \times \frac{\boldsymbol{\lambda_g}}{\boldsymbol{\lambda}} \quad (3.9)$$

From (3.8) and (3.14), the guide impedance of TE mode of the SIW in Fig 3.3 at 25GHz is calculated to be 38 Ω. Based on the calculated guide impedance, the transition from 50 ohm microstrip line to 38 ohm microstrip line can be optimized by both calculation and simulation. Table 3.2 shows the calculated line widths of a 50 ohm microstrip line and a 38 ohm microstrip line and a quarter wavelength transition length at 25GHz.

Table 3.2 Calculated parameters for microstrip impedance transition

50 ohm Microstrip Line width	*w1*	0.55mm
38 ohm Microstrip Line width	*w2*	1.25mm
Transition length	*L*	1.8mm

Based on the calculated parameters in Table 3.2, the transition model of 50 ohm microstrip to the designed SIW is drawn in Fig. 3.5

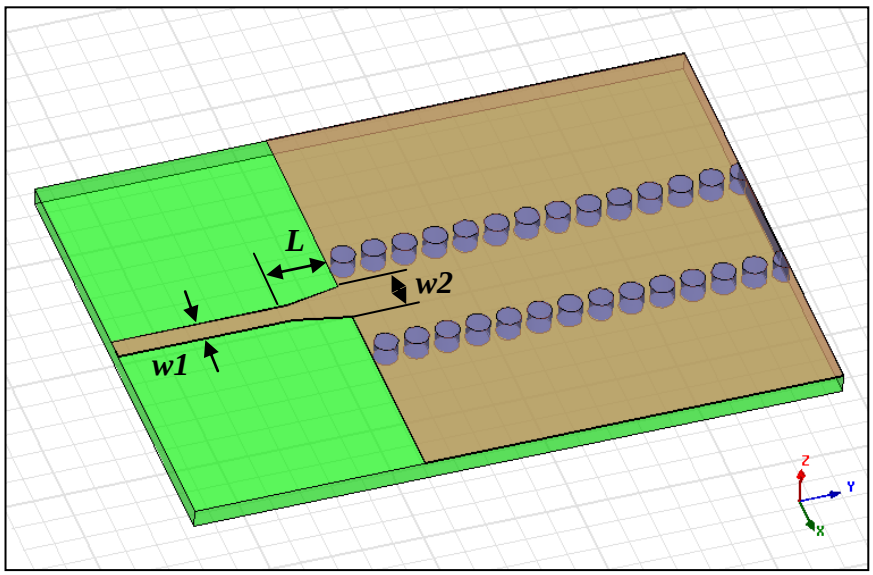

Fig. 3.5 Transition model of Microstrip to SIW

Figure 3.6 presents the simulated result of the transition model. Therein, more than 20dB return loss over the frequency band of 22GHz to 26GHz has been achieved. From the simulation, though a better result can be achieved when the first via is located right on the edge of upper ground edge, the first via hole is placed at 10mil away from the upper ground edge limited by our PCB fabrication.

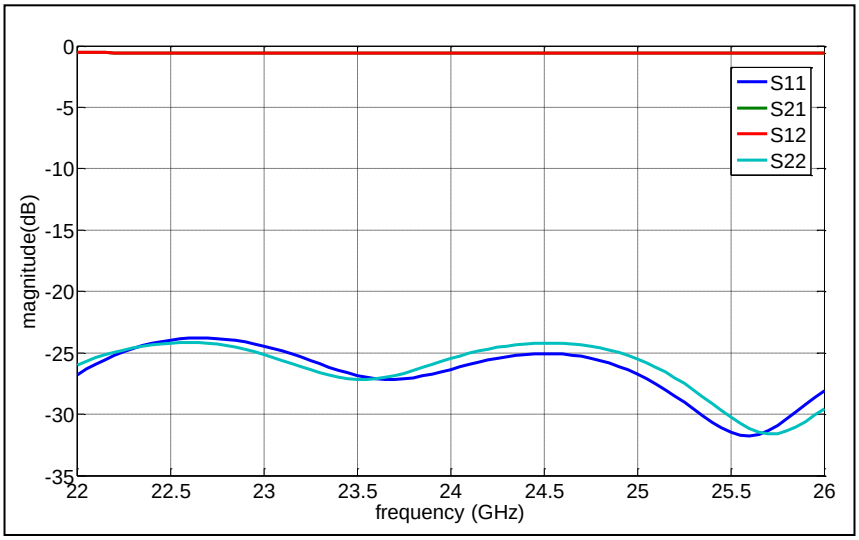

Fig. 3.6 Simulated result of the optimized transition model

As the next step, as SIW back to back model, which will be used as the base for the design of Ferrite phase shifters in this thesis, has been designed and fabricated. Figure 3.7 shows the simulation model and the fabricated model of the SIW with the back to back transition.

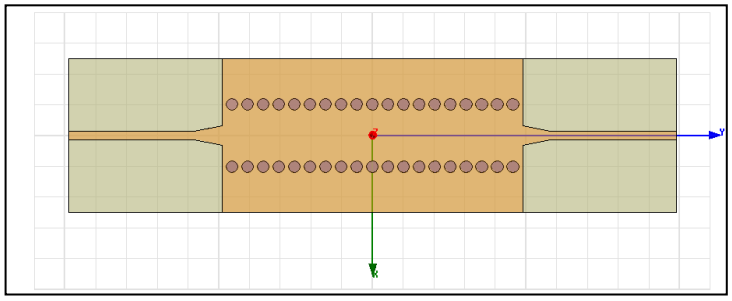

(a) Simulation model

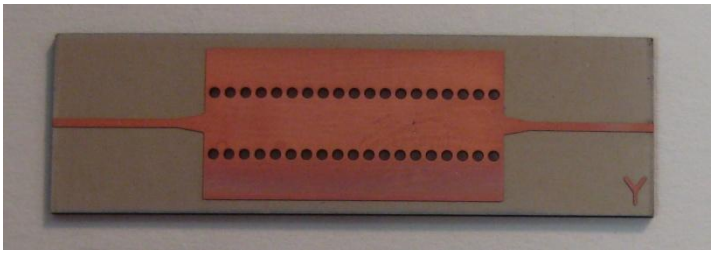

(b) Fabricated SIW

Fig. 3.7 SIW with back-to-back connection

For accurate measurements, a TRL calibration kit has been also fabricated as shown in Fig. 3.8 using the 50ohm line configuration in Table 3.2.

Fig. 3.8 TRL calibration kit

Figure 3.9 shows the comparison between the simulated result of Fig 3.6 (a) and the measured result of Fig 3.6 (b). Both the simulated return loss and the measured return loss are better than 18dB for the frequency range from 22GHz to 26GHz. The insertion losses in both simulated and measure results are less than 1.0dB over the frequency range.

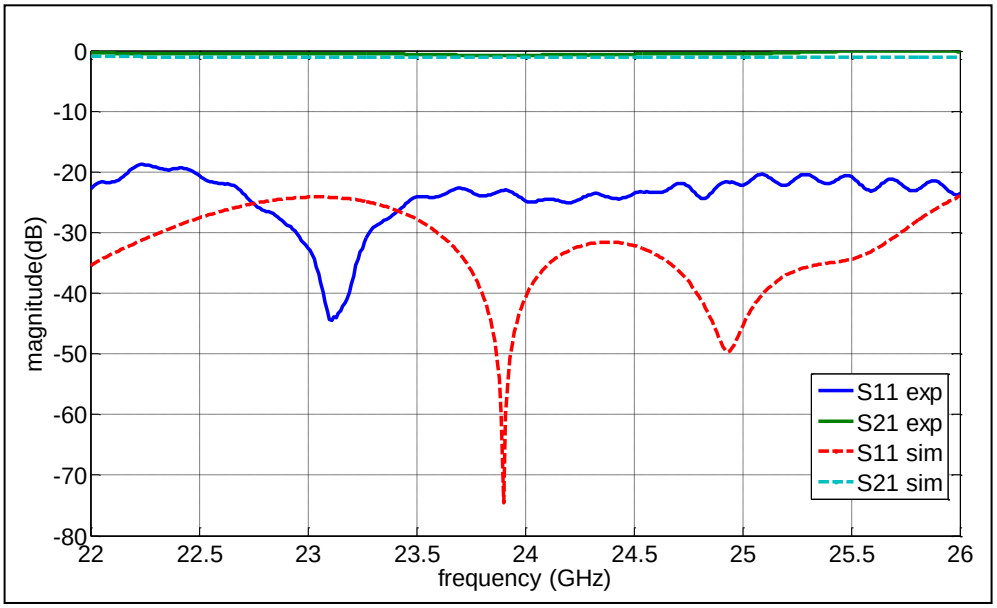

Fig. 3.9 Measured and simulated results of return loss and insertion loss of the SIW back-to-back transition

3.7 Conclusion

Based on rectangular waveguide theory, specific design rules of SIW for the design of via-hole array and effective width of broad side wall among others were reviewed. The cut off frequency was deliberately selected to avoid higher-order modes while maximizing the broad side width and a SIW was modeled and simulated out of Roger 25mil 6010 material using the SIW design rules described in this chapter. For transition from microstrip to SIW, guided-wave impedance of SIW was calculated in order to decide the matched width of mircostrip, then simulations and experiments were followed up to verify the matching condition. Thus, the designed SIW in this chapter will be used as a base of the following ferrite phase shifters.

CHAPTER 4

SINGLE FERRITE SLAB PHASE SHIFTER USING SUBSTRATE INTEGRATED WAVEGUIDE TECHNIIQUE

4.1 Introduction and modeling

In Chapter 2, the propagation of plane waves in an infinite ferrite medium was explained. However, in practice, plane waves propagate in finite waveguides or other types of transmission lines. From the perturbation theory, Clarricoats has derived expressions containing nonreciprocal terms, showing that the wave travelling through the rectangular waveguide suffers from different phase shifts depending on the direction of propagation [19]. In this chapter, a ferrite material is placed at a specific position in rectangular waveguide and a circular polarization is presented.

There are natural regions of circular polarization in rectangular waveguide that operates in TE_{10} Mode. When ferrite slabs are placed in these regions, waves with circular polarization are excited in the ferrite because the circularly polarized plane wave rotating in the same direction as the precessing magnetic dipole has a strong interaction with the ferrite material. The sense of polarization (left or right hand) depends on the direction of wave propagation in the waveguide. Waves travelling in the forward direction in the waveguide excite circular polarized waves in the ferrite with one sense of polarization, and waves travelling in the reverse direction excite waves in the ferrite with the opposite sense of polarization. [20].

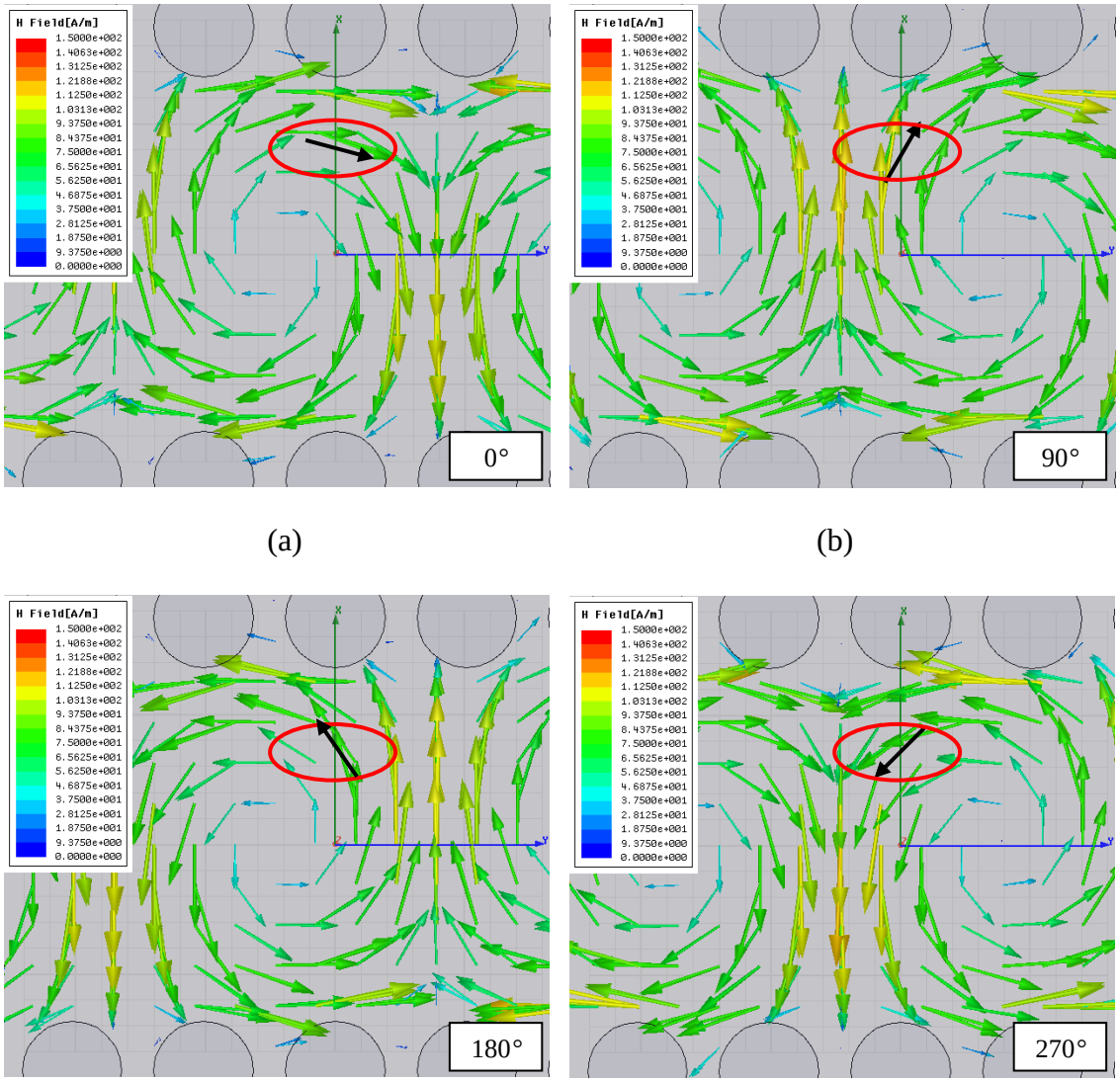

(a) (b)

(c) (d)

Fig. 4.1 Magnetic field propagation and the circular polarization at one forth location in Substrate Integrated Waveguide

As the propagation constant of the wave travelling in one direction becomes different from that of the wave travelling in the opposite direction caused by different circular

polarization, there are different phase shifts associated with the transmission of the two types of waves in the ferrite-loaded waveguide.

As a wave travels down the guide, the magnetic field lines also travel. Fig 4.1 shows there are regions of circular polarization in rectangular waveguide. If we consider the direction and magnitude of the magnetic field at a particular position and instant of time, it can be observed that a field vector rotates as shown in Fig 4.1. As time progresses, the field vector rotates due to the change in the magnetic field. At a certain position in the waveguide, the magnitude of the magnetic field vector does not change; only the direction changes and we have circular polarization. Circular polarization occurs at a point in the guide about one quarter of the wave across. The sense of polarization is opposite for waves traveling in opposite directions in the waveguide. [20]

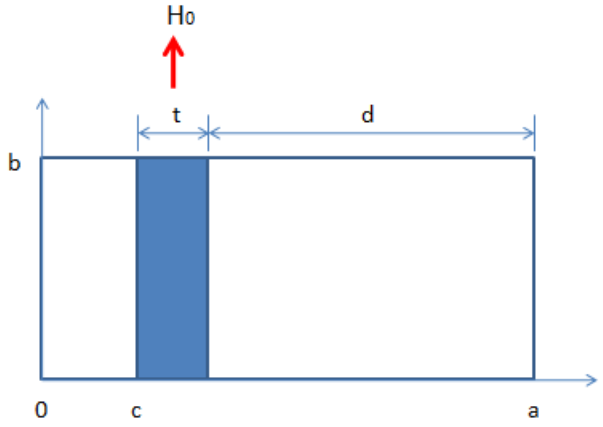

Fig. 4.2 Geometry of a rectangular waveguide loaded with a transversely biased ferrite slab [21]

When a ferrite slab is loaded into a waveguide, the geometry and the magnetic field distribution become complicated. A transcendental equation for the propagation constant β is given by

$$\left(\frac{k_f}{\mu_e}\right)^2 + \left(\frac{\kappa\beta}{\mu\mu_e}\right)^2 - k_a \cot k_a c \left(\frac{k_f}{\mu_o\mu_e} cot k_f t - \frac{\kappa\beta}{\mu_o\mu\mu_e}\right) - \left(\frac{k_a}{\mu_o}\right)^2 \times \cot k_a c \cot k_a d - k_a \cot k_a d \left(\frac{k_f}{\mu_o\mu_e} cot k_f t + \frac{\kappa\beta}{\mu_o\mu\mu_e}\right) = 0 \quad (4.1)$$

where k_f is a cutoff wavenumber for the ferrite and k_a is a cutoff wavenumber for dielectric SIW region and dimensional parameters of c, d and x are indicated in Fig.4.2 [22].

The approximate result for the differential phase shift, ($\beta^+ - \beta^-$), through the perturbation theory is given by

$$\beta^+ - \beta^- = \frac{2\pi d}{a^2}\frac{\kappa}{\mu} sin\frac{2N\pi x}{a} \quad (4.2)$$

where *N* is an integer. The maximum differential phase shift is obtained when $x = a/4$.

The ferrite slab thickness used in this thesis is considered too thick to apply the approximation equation given by Pozar [23]. However, it is useful to understand the physical meaning of the geometry.

The approximation gives us the information that a larger phase shift can be achieved when the ferrite slab is located in near $a/4$ position even though it is based on the assumption that the ferrite thickness is very thin compared with the waveguide width. The position should be adjusted experimentally to obtain a good differential phase shift

and, more importantly, minimum variation in phase shift over the frequency band of interest.

Table 4.1 shows design parameters for the single slab ferrite phase shifter using SIW technique. For the simulation, a Nickel ferrite which has 5000 Gauss of saturation magnetization is chosen and the material parameter is detailed in Table 2.1.

Table 4.1 Design parameter of Substrate Integrated Waveguide

SIW width	a	4.064mm
Effective width	a_{eff}	3.448mm
Via hole diameter	d	0.77mm
Gap between via holes	g	1.016
Ferrite offset from the wall	c	0.4mm
Ferrite slab length	l	12.7mm
Ferrite slab width	t	0.762mm
Ferrite slab thickness	h	0.762mm
SIW length	$l2$	20mm
Substrate thickness	b	0.635mm

In order to verify the excitation of circular polarization with 0.4mm offset from the wall, magnetic field vector distribution in the ferrite slab is displayed in Fig 4.3. Figure 4.3(a) shows a strong excitation of circular polarization that is generated for the wave travelling to one direction, whereas Figure 4.3(b) shows that a weak excitation is observed for the wave travelling in the opposite direction.

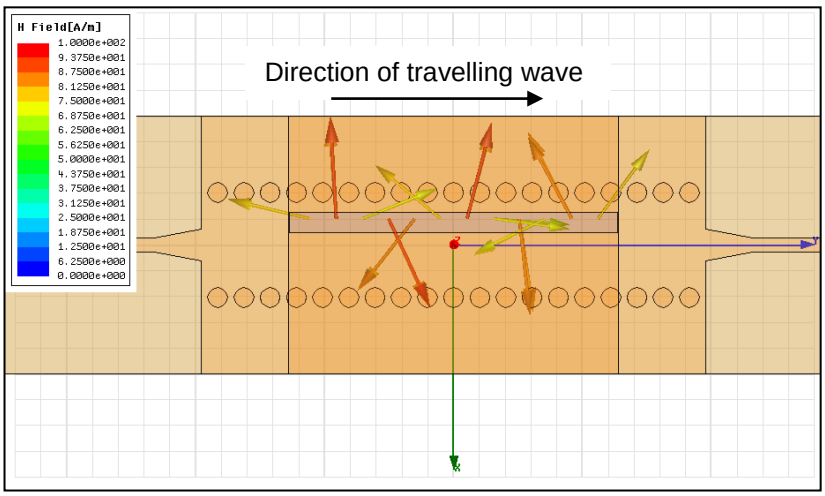

(a)

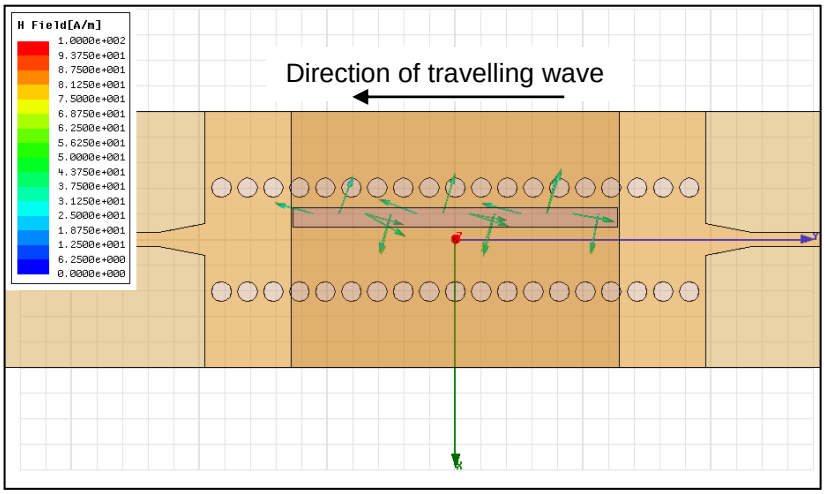

(b)

Fig. 4.3 (a) The magnetic field in forward travelling wave shows a strong excitation in the ferrite which is transversely magnetized to the z direction (b) The magnetic field in the reverse travelling wave shows a weak excitation in the ferrite which is transversely magnetized to the z direction

With the design parameters given in Table 4.1 and the offset model shown in Fig.4.3, a single ferrite slab phase shifter using Substrate Integrated Waveguide technique is modeled as shown in Fig.4.4. The simulated result of the model in Fig.4.3 will be discussed in section 4.3 together with the measured result.

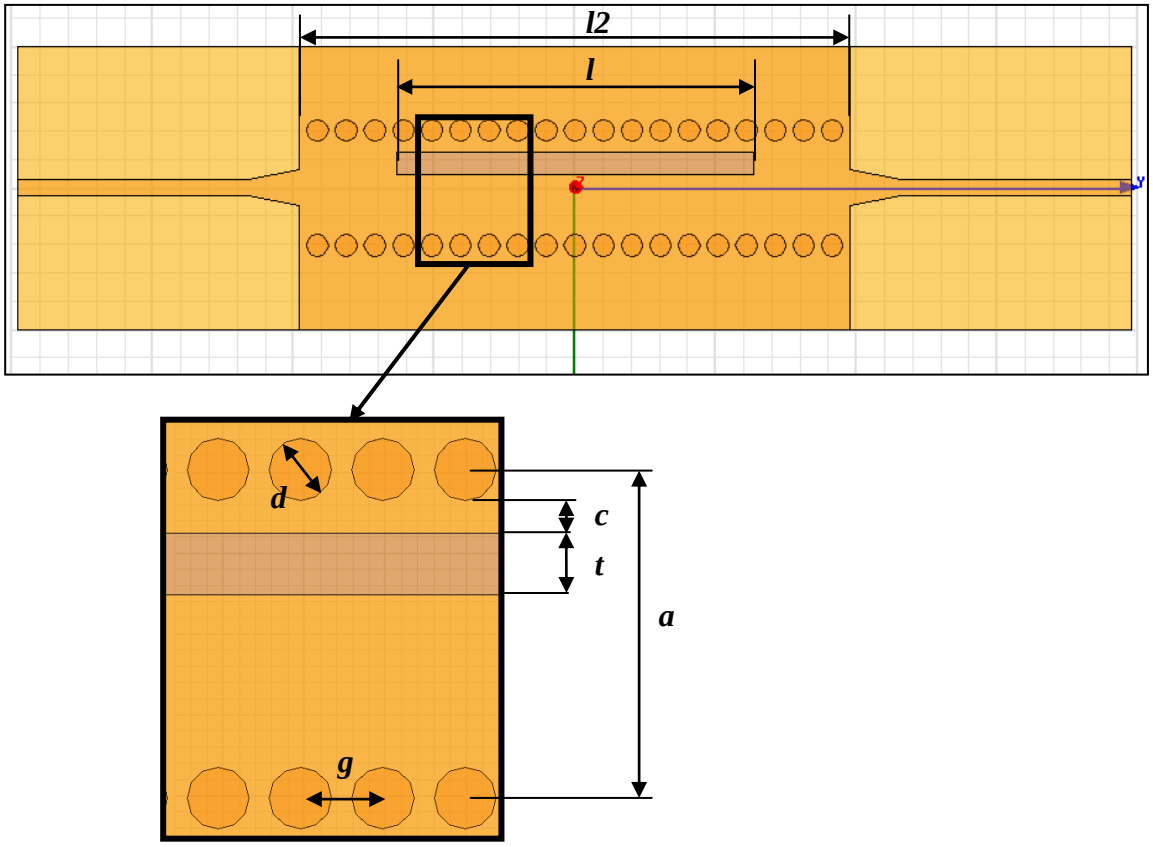

Fig. 4.4 Top view of single slab ferrite phase shifter using Substrate Integrated Waveguide

4.2 Fabrication and ferrite magnetization

For the experimentation of ferrite phase shifters using SIW technique, two ferrite materials are prepared. One is Nickel ferrite as described in Table 2.1 and the other is Lithium ferrite that was described in Table 2.2. Nickel ferrites have a high saturation magnetization value which is optimal for high frequency applications and Lithium ferrites have a high residual magnetization value which is optimal for latching ferrite phase shifter applications. While machining those ferrites to the slabs, we can notice that Lithium ferrite materials are too brittle to machine into a thin ferrite slab which has 0.762mm width as per the design in Table 4.1. Even though several trials were given for the machining of Lithium ferrites, it was not possible to machine Lithium ferrite slabs in our Poly-Grames Research Center. Therefore, only Nickel ferrite materials were machined and applied to the design of the proposed phase shifters in this thesis.

For the fabrication of Substrate integrated waveguide, Rogers RT/Duroid 6010 substrate was used with the design parameters as shown in Table 4.1. After the SIW was fabricated, a slot having the same dimensional size as the machined ferrite slab was machined to accommodate the ferrite slab. Fig 4.5 shows the machined Nickel ferrite slab and fabricated substrate integrated waveguide that has a machined open slot.

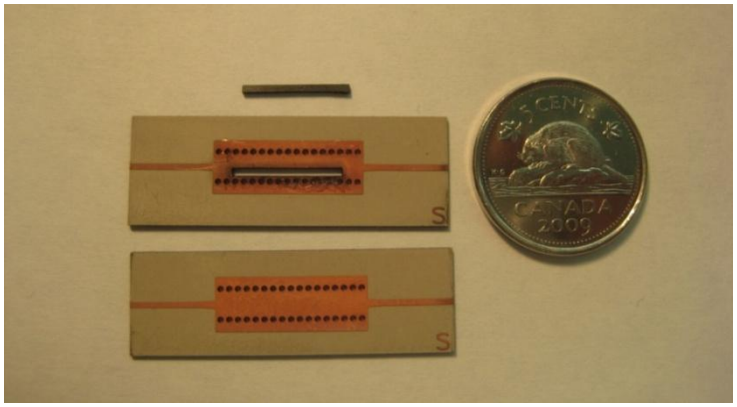

Fig. 4.5 Fabricated SIW and ferrite

Once the ferrite slab in Fig 4.5 was inserted into the open slot in the SIW, a conductive copper foil tapes were applied on both top and bottom planes to close the waveguide broad walls. During our preliminary measurements of the completed ferrite phase shifter, it was observed that the measured result was quite unstable and very far from the simulated result. Through several experiments, it was found that there was some electro-magnetic field leakage through the conductive glue layer, and the leakage led to such a large discrepancy between simulated and measured results. To solve the problem, the conductive copper foil tape was resized to be slightly larger than the ferrite slab and then soldering was applied around the conductive tapes so that the applied solder can fully cover the gap between the SIW open slot and the conductive copper foil tape. Finally, a reasonable experimental test result, which agreed with the simulated result, was obtained.

In order to magnetize the single ferrite slab in the SIW phase shifter, an electromagnet system was used. The single slab ferrite phase shifter was positioned in

between two electromagnet cores. Figure 4.6 shows the experimental setup. The SIW ferrite phase shifter is inserted into the electromagnet system. S-parameters are captured using the connected VNA while measuring the applied external magnetic field at the same time using a Gauss Meter putting near the ferrite phase shifter.

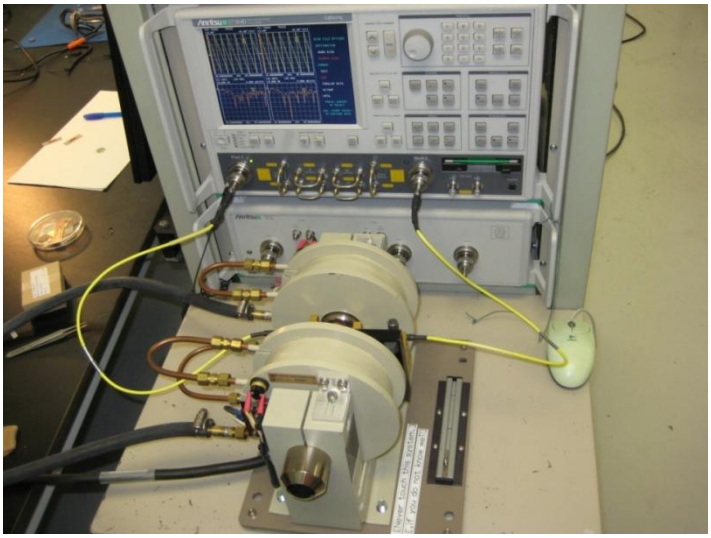

Fig. 4.6 Experimental setup for characterization of the ferrite phase shifter

As shown in Fig. 4.7 a test fixture was used and inserted between the two electromagnet cores to measure S-parameters of the SIW ferrite phase shifter. However, because the size of the fixture was too large compared with the electromagnet cores, the gap between the two electromagnet cores became significantly large, and accordingly it increased the magnetic reluctance like a large air gap. Therefore, the external magnetic field generated by the electromagnet was not enough to see the point where the effective permeability had “zero” value which was shown in Fig 2.6.

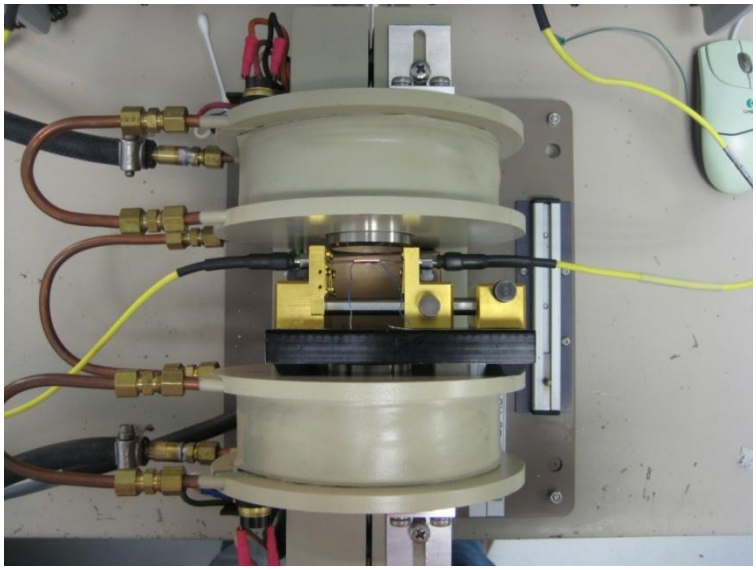

Fig. 4.7 Ferrite phase sifter located in an electromagnet system

4.3 Simulated and Measured Results

Figure 4.8 shows both measured and simulated return loss results of the single ferrite slab phase shifter without an external magnetic field. It is observed that more than 20dB return loss matching condition can be achieved in simulation and better than 15dB return loss in measurement. The difference between the simulated and measured results may come from a small air gap between the ferrite slab and the open slot in SIW as well as an imperfect shielding of the broad walls made of the copper foil tapes. It is also observed that the insertion losses in both simulated and measured results are smaller than 1.5dB.

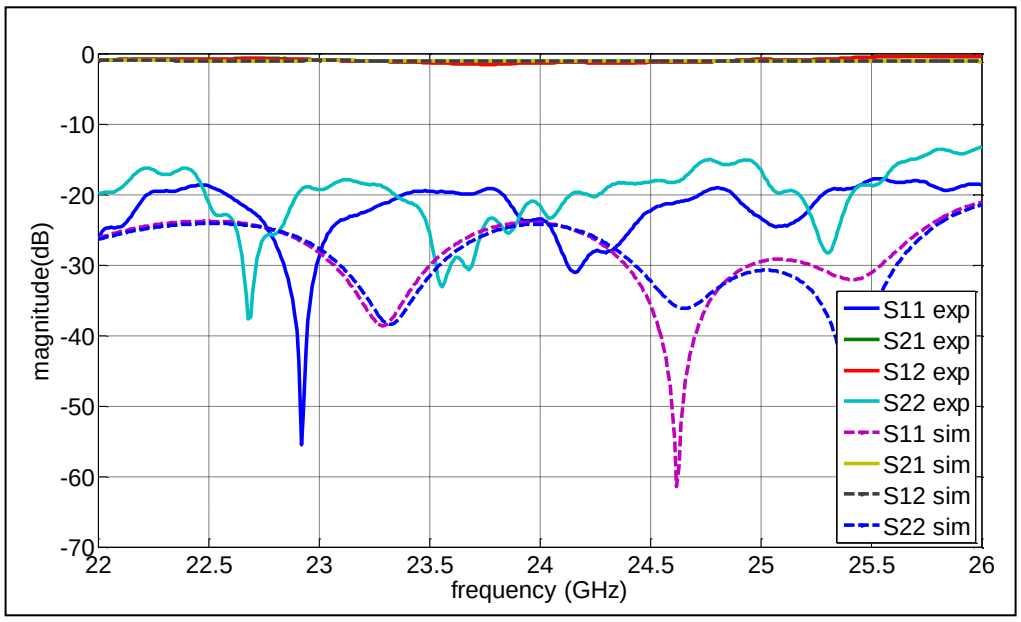

Fig. 4.8 Measured and simulated results of SIW single slab ferrite phase shifter without external magnetic field application

As compared with Fig. 4.8, Fig. 4.9 shows both measured and simulated matching results of the single ferrite slab phase shifter when the ferrite slab is magnetized to saturation. There is no significant difference in the matching results observed between the unmagnetized ferrite phase shifter and the magnetized ferrite phase shifter. This is because the effective permeability of the ferrite material is changed when the external magnetic field is changed over the ferrite phase shifters as previously shown in Fig 2.6, the matching results of phase shifter can be significantly affected by the amount of magnetization of the ferrites in the phase shifter. Therefore, the ferrite phase shifters should be designed with the consideration that the matching result should be consistently acceptable in a given variation of the applied magnetic field bias.

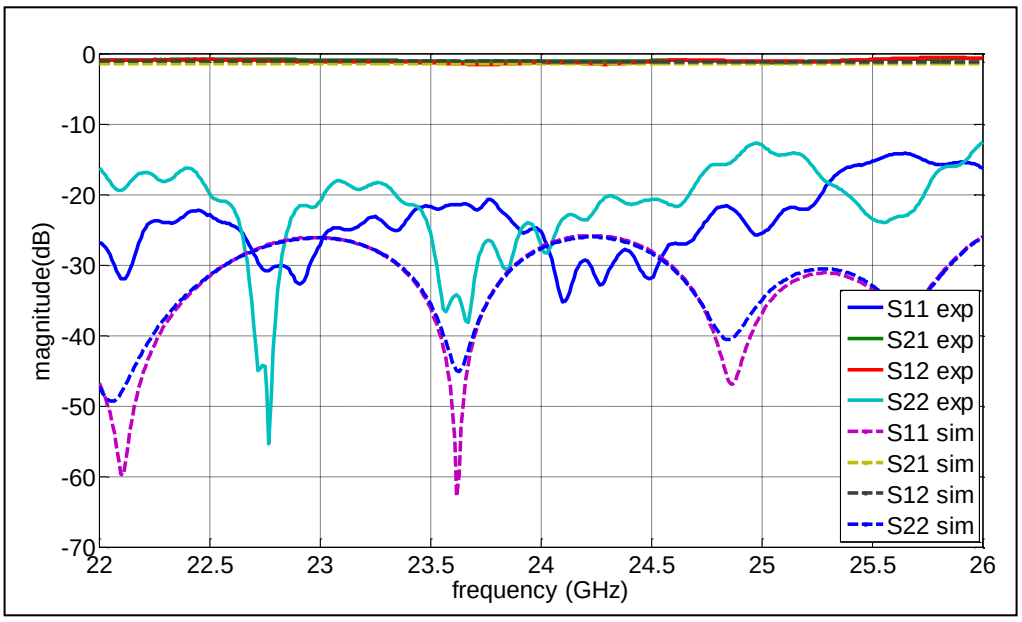

Fig. 4.9 Measured and simulated results of SIW single slab ferrite phase shifter with fully magnetized ferrite slab

Regarding the evaluation of the saturation magnetization, it is also important to understand the relationship between the external magnetic field and the internal magnetic field. This is because a demagnetization caused by the shape of ferrite material makes that the magnetic field strength inside the ferrite is different from the magnetic field generated between the two electromagnet cores. The relationship is given by

$$H_i = H_0 - N_z M \tag{4.3}$$

where N_z is the shape demagnetizing factor in z direction.

The shape demagnetizing factor for the ferrite slab can be approximately calculated to be 0.5 as the slab is long enough compared with its width and its thickness as described in Table 4.1 [24]. As the saturation magnetization of Nickel ferrite in this

phase shifter is 5000 Gauss, it can be assumed that an external magnetic field of 2500G would be required to fully magnetize the ferrite slab to saturation. Therefore, the measured result in Fig 4.9 was captured under the assumption that 2500G external magnetic field can fully magnetize the ferrite slab in the phase shifter. Thus, the internal magnetic field intensity H_i becomes zero.

Fig. 4.10 describes both measured and simulated phase values of S21 and S12 by the change of applied external magnetic field bias. As the external magnetic field increases, both S21 phase and S12 phase start splitting from each other. One interesting observation is that not only S21 phase, which is the phase in the forward propagation direction, but also S12 phase, which is the phase in the reverse direction, are changed by the change of external magnetic field intensity. Another interesting observation is that measured S12 phase shows a linear decrease until the external magnetic field reaches to around 2000 Gauss, then the S12 phase starts being saturated, whereas the simulated S12 phase shows a linear decrease until exact 2500 Gauss, then gets saturated. It shows that it requires about 2000 Gauss external magnetic field intensity to make the ferrite slab magnetized to the saturation. It means that the actual shape demagnetizing factor in the single ferrite slab phase shifter may be about 0.4 according to (4.3)

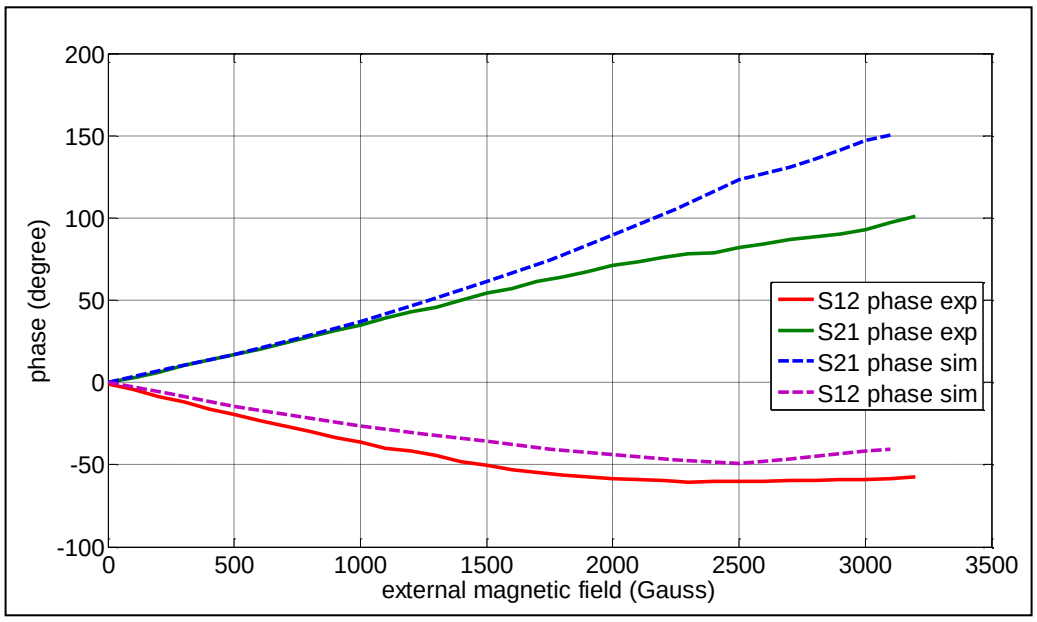

Fig. 4.10 Measured and simulated results of phase split between S21 and S12 at 24GHz

From the phase splitting variation between S21 and S12 in Fig. 4.10, it is possible to calculate the resulting phase shift of the designed single ferrite slab phase shifter. Fig. 4.11 presents the differential phase shift values in both measured and simulated results. About 190° of differential phase shift has been achieved in simulation with 3200G external magnetic field intensity and about 160° of differential phase shift is achieved in experiment with 3200G external magnetic field intensity. As mentioned above, more phase shift could be obtained if more external magnetic field intensity were applied to the designed ferrite phase shifter. However, there was a limitation to increase the external magnetic field intensity because of a very large gap between the electromagnet cores as shown in Fig. 4.7.

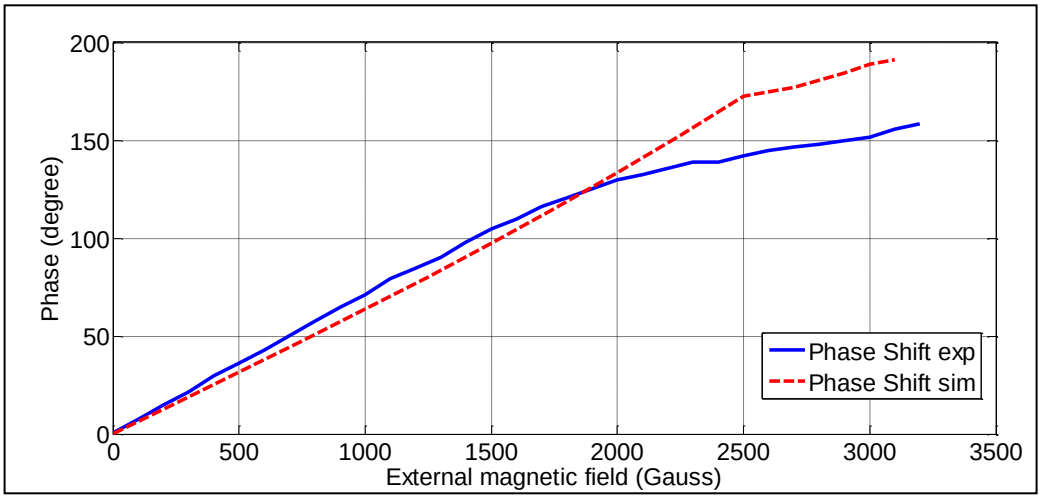

Fig. 4.11 Measured and simulated results of differential phase shift at 24GHz

Fig. 4.12 shows the insertion loss variation by changing the applied external magnetic field. The simulated result shows that the insertion loss of S21 increases as the external magnetic field increases, whereas the insertion loss of S12 does not change significantly by changing the external magnetic field intensity. The excitation of circular polarization in one direction is increased when the external magnetic field intensity increases whereas the circular polarization in the opposite direction is not excited significantly. Thus, the increased amount of circular polarization in one direction increases the loss which is described as the imaginary part of effective permeability of the applied ferrite slab. However, the measured insertion loss result in Fig 4.12 shows that a loss in S21 is relatively consistent with the change of the external magnetic field intensity. It seems that the variation of input matching results over the external magnetic field gives a more impact on the insertion loss than the impact the magnetic loss can give.

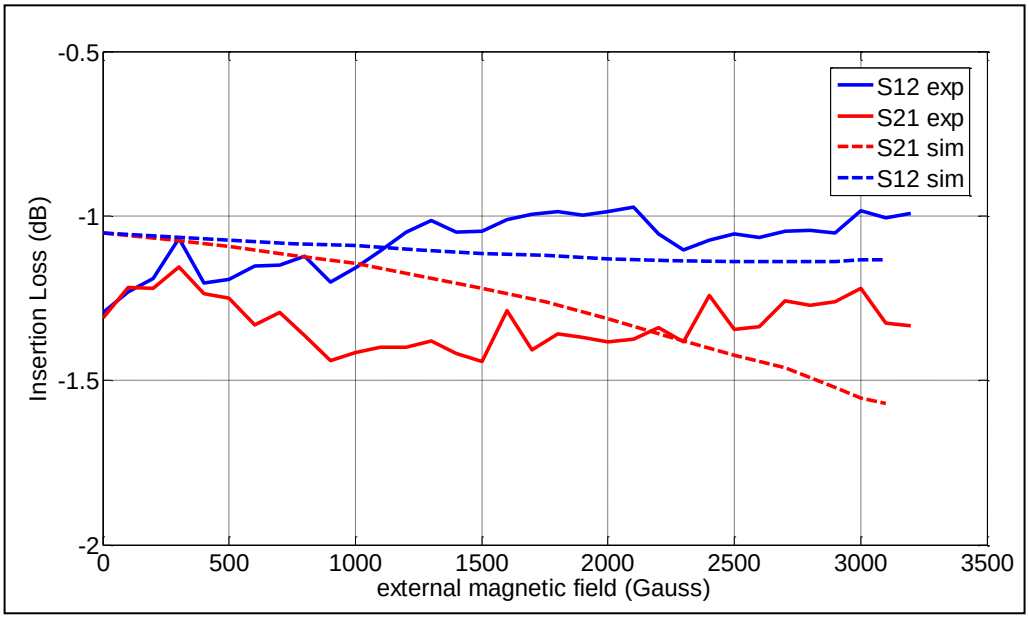

Fig. 4.12 Measured and simulated results of insertion loss at 24GHz

4.4 Conclusion

The return loss of the phase shifter in this chapter was better than 15dB and the insertion loss was better than 1.5dB. Shape Demagnetization Factor was introduced and its value of the ferrite slab was calculated and compared. For magnetization of the ferrite slab in the phase shifter, an electromagnet was used. The internal magnetic field was calculated based on the external magnetic field generated in between the two electromagnet cores and the shape demagnetization factor. The measured shape demagnetization factor of the ferrite slab was about 0.4. The achieved phase shift in both simulation and experiment was more than 150°.

CHAPTER 5

DOUBLE FERRITE SLAB PHASE SHIFTER USING SUBSTRATE INTEGRATED WAVEGUIDE TECHNIQUE

5.1 Introduction and Modeling

To begin with, let us look at a useful geometry is the rectangular waveguide loaded with two symmetrically placed ferrite slabs, as shown in Fig. 5.1. With equal but opposite transversely directed bias fields on the ferrite slabs, this configuration provides an interesting model for the nonreciprocal phase shifter.

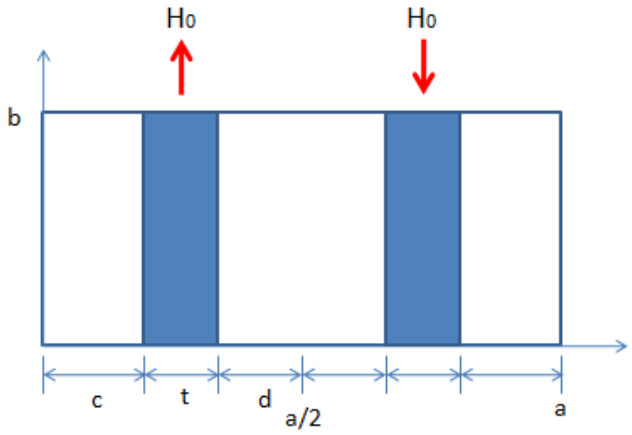

Fig. 5.1 Geometry of a rectangular waveguide loaded with two symmetrical ferrite slabs [25]

The analysis of such a double slab ferrite phase shifter is very similar to that of the single slab geometry because the ferrite slabs on the opposite sides of the waveguide are magnetized in the opposite direction, both ferrite slabs present the same permeability to

the wave in the waveguide and the field is symmetrical. A transcendental equation for propagation constant β is given by [26]

$$\left(\frac{k_f}{\mu_e}\right)^2 + \left(\frac{\kappa\beta}{\mu\mu_e}\right)^2 - k_a \cot k_a c \left(\frac{k_f}{\mu_o\mu_e} cot k_f t - \frac{\kappa\beta}{\mu_o\mu\mu_e}\right) + \left(\frac{k_a}{\mu_o}\right)^2 \times \cot k_a c \tan k_a d - k_a \tan k_a d \left(\frac{k_f}{\mu_o\mu_e} cot k_f t + \frac{\kappa\beta}{\mu_o\mu\mu_e}\right) = 0 \quad (5.1)$$

The above characteristic equation yields a relationship between the dimensions of the ferrite, waveguide and the propagation constant for a specified set of ferrite parameter values.

As the direction of circular polarization is opposite on the opposite sides of the waveguide, two ferrite slabs magnetized in opposite directions on the opposite sides of the waveguide can give the most efficient phase shift. Fig. 5.2 shows the designed geometry of the SIW ferrite phase shifter with two symmetrically located ferrite slabs. For this design, one more ferrite slab is added on the opposite side of the waveguide judging from the geometry of a single ferrite slab phase shifter in Fig 4.4.

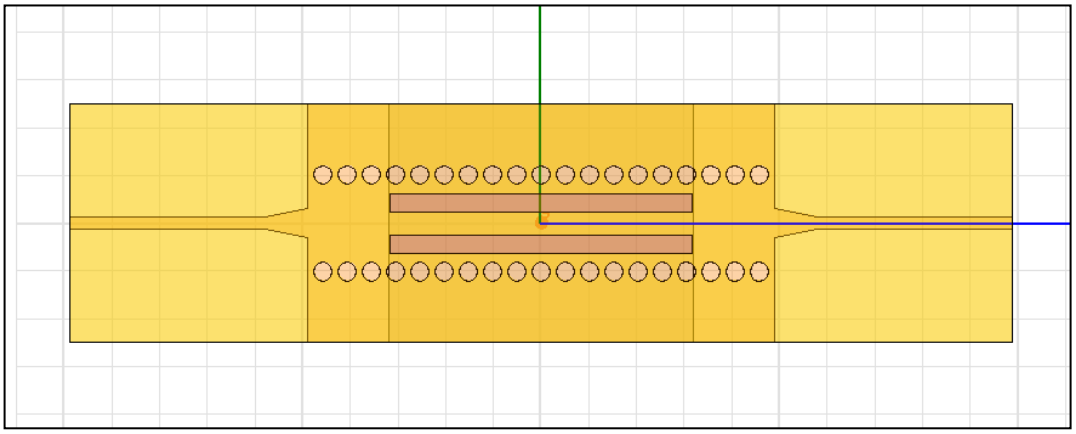

Fig. 5.2 Geometry of double ferrite slab phase shifter using SIW technique

Fig. 5.3 shows simulated results of the phase shifter described in Fig. 5.2. S-parameters of the phase shifter without magnetization of the ferrite slabs are compared with S-parameters of the phase shifter with the ferrite slabs which are fully magnetized to saturation. In both cases, a better than 20dB matching condition was observed, and this was better than the case of the single ferrite slab phase shifter in the previous chapter.

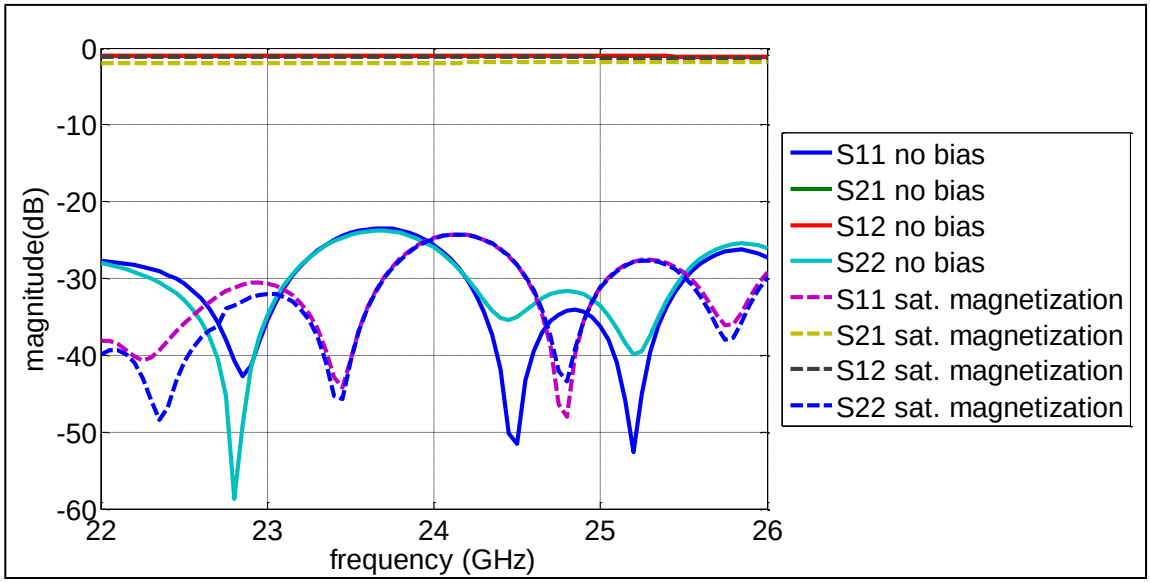

Fig. 5.3 Simulated results of double ferrite slab phase shifter using SIW technique in both without external magnetic bias and with external magnetic bias to full saturation magnetization

Fig. 5.4 shows the simulated results of phase split by the change of magnetization of the ferrites. For this simulation, a transverse magnetization was applied in one direction to one ferrite slab and the opposite transverse magnetization was applied to the other ferrite slab. A parametric sweep of saturation magnetization value from 0 to 5000G through HFSS simulation package is conducted under the assumption that there is no

internal magnetic field in the ferrite materials until the magnetization reaches to saturation magnetization. As the frequency of interest is ranging from 22GHz to 26GHz, the phase split variations at 22GHz, 24GHz and 26GHz are compared together in Fig. 5.4. The result shows that a more phase split can be achieved as frequency becomes lower when the saturation magnetization of the ferrite used is constant. The phase split behavior in Fig. 5.4 is similar to that in Fig. 4.10 when two figures are compared only over the below saturation magnetization range. However, as easily predicted, the phase split amount at the double ferrite slab phase shifter in Fig. 5.4 is much larger than that of the single ferrite slab phase shifter in Fig. 4.10.

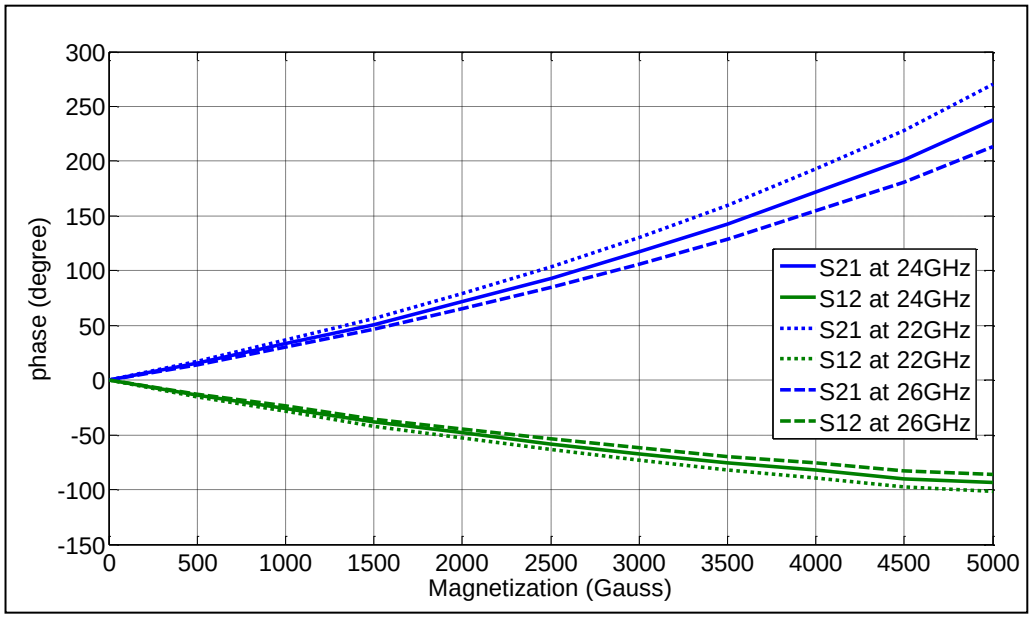

Fig. 5.4 Simulated results of phase split between S21 phase and S12 phase

Fig. 5.5 shows the resulting phase shift variation calculated from the phase split in Fig. 5.4. As expected from Fig. 5.4, the phase shift result in Fig. 5.5 shows that the

differential phase shift value is linearly increased over the magnetization change. At the saturation magnetization of 5000G, more than 300° differential phase shift is achieved in simulation.

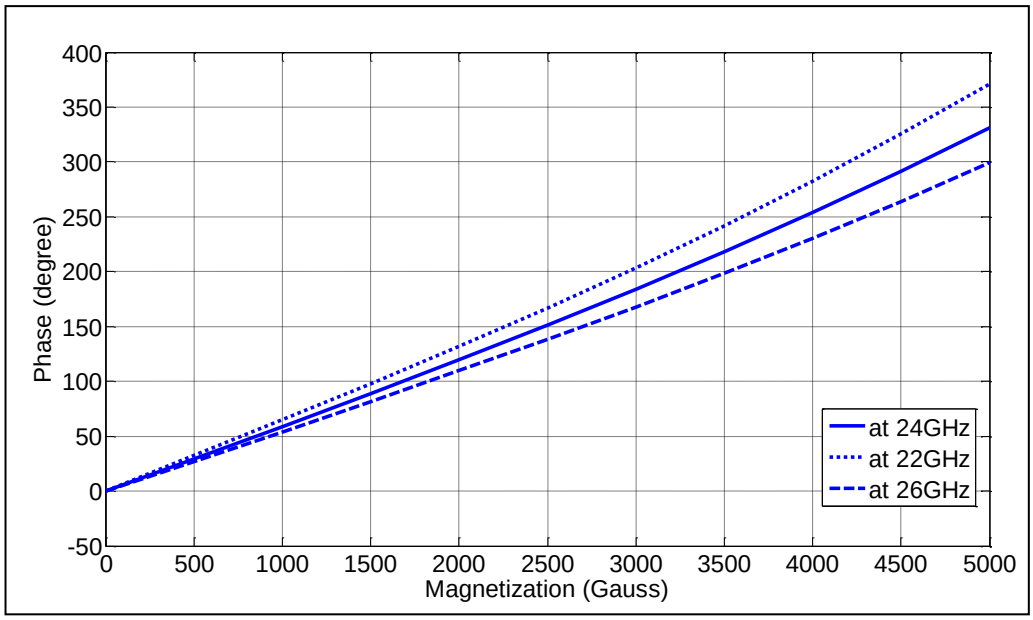

Fig. 5.5 simulated results of differential phase shift

Fig. 5.6 shows the insertion loss variation over the magnetization change. The result shows that more insertion loss takes place at S21 than S12. As explained in Chapter 4, a more excitation of circular polarization in the forward direction gives rise to a more magnetic loss at the forward direction accordingly. However, in practice, “low-field loss” should be considered. This low-field loss cannot be simulated in HFSS package. As opposite to the simulation result in Fig. 5.6, the low-field loss may be larger at the low magnetization. When ferrite material is unmagnetized or magnetized below saturation, each crystal is split up into a number of domains, and magnetized to saturation but in

arbitrary directions other than unilateral transverse direction. These arbitrary magnetizations generate unpredictable resonance loss in the material. If the ferrite is magnetized to saturation, there is no longer any possibility of change of direction of the anisotropy field or of domain wall, thus this resonance does not occur [2].

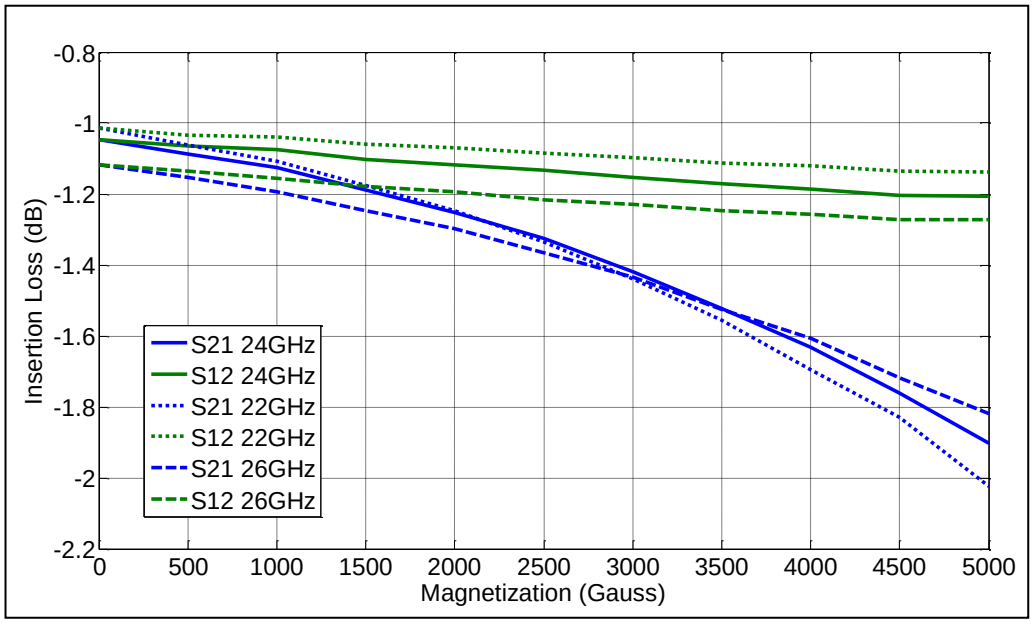

Fig. 5.6 simulated results of insertion loss at 22GHz, 24GHz and 26GHz

5.2 Fabrication and Ferrite Magnetization

As explained in Chapter 4, at the beginning, two ferrite materials were prepared for the ferrite phase shifter for comparison purpose. One was Nickel ferrite in Table 2.1 and the other was Lithium ferrite in Table 2.2. However, it was impossible to machine Lithium ferrite because Lithium ferrite was too brittle to machine. Thus, a ferrite phase shifter using Lithium ferrite was not fabricated in this thesis. Only Nickel ferrite was

used for experiments. Two Nickel ferrite slabs were machined with the dimensions shown in Table 4.1.

For the fabrication of SIW for the double ferrite slab phase shifter, the same laminate material, which is Rogers RT/Duroid 6010, was used with also the same dimensions in Table 4.1. The only difference is that one additional slot was machined in the SIW so that two ferrite slabs could be inserted into the SIW with a dimensional symmetry to each other. After the SIW fabrication was completed, two machined ferrite slabs were inserted into the two open slots.

For magnetization of the ferrite phase shifter, a closed magnetic field loop system was devised as shown in Fig. 5.7. A rectangular shape of steel plate, which is made of a ferromagnetic material, was placed on top of the SIW broad wall so that it can provide a shunt path of static magnetic field as well as an electrical ground plane of the open broad wall. For the bottom opening of the SIW, a long steel plate was prepared and shaped to omega form. The distance between both ends of the omega shape plate was adjusted to be the same as the spacing between the two ferrite slabs. And each steel plate was prepared with silver plating so that it can accept soldering.

Before the omega shape plate was soldered to the bottom of the SIW, coil was wound around the plate so that a magnetization of both ferrite slabs could be achieved through applied DC current to the coil wound around the omega plate. As the space between the two ferrite slabs was only 0.97mm, it was necessary to shape the steel plate to be omega in order to maximize the space for winding of the coil. Thus, as shown in Fig. 5.7 (b), a closed magnetic field loop was achieved using the two steel plates and the two ferrite

slabs. Once DC current is applied to the coil, static magnetic field is generated in the omega shape plate which works as a magnetic core, and then the two ferrite slabs can be magnetized in opposite direction to each other.

When the closed magnetic field loop was implemented, the ferrite thickness was designed a little thicker than the thickness of the laminate material as shown in Table 4.1 in order to minimize any possible magnetic reluctance caused by air gap between the ferrite slabs and the steel plates. And the two cutting faces of the omega shape plate were polished well to be flat.

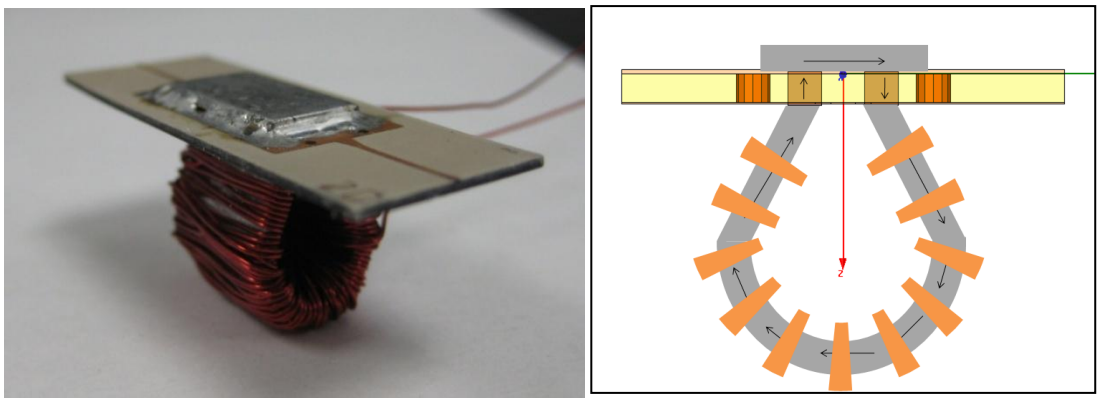

(a) Experimental sample (b) simplified cutting view

Fig. 5.7 Ferrite phase shifter with magnetic biasing system

However, during our experiments, it was found that the number of turns of the coil was not enough to magnetize the ferrite as much as we anticipated. Therefore, the closed magnetic loop was redesigned as shown in Fig. 5.8. In order to increase the number of turns, a thinner coil was wound around the omega plate. In addition to that, the top steel plate was replaced to another omega shape steel plate. A very thin wire, which has 0.07mm in diameter, was wound around each omega shape plate by 750 turns. Figure

5.8(b) shows the simplified cutting view of the completed double ferrite slab phase shifter having two coil systems. Of course, each coil was wound in the direction to double the static magnetic field in the closed magnetic loop.

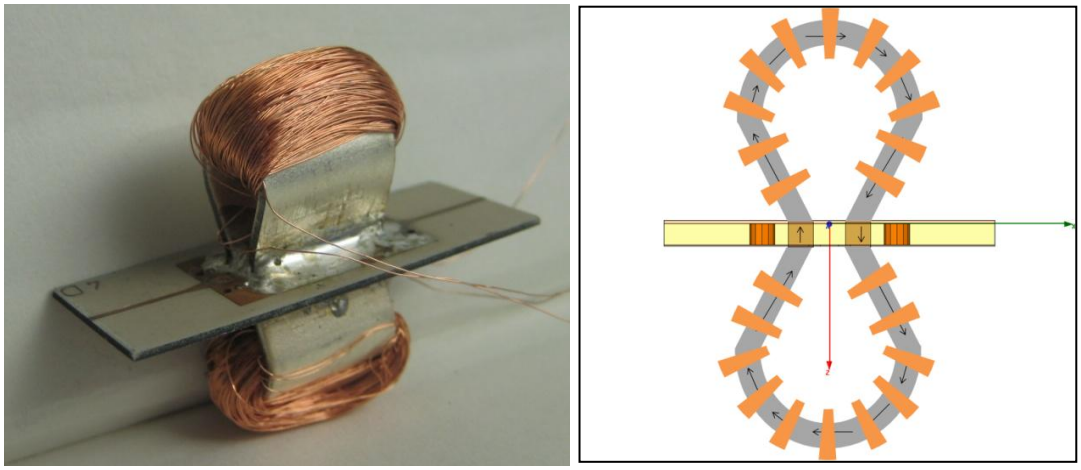

(a) Experimental sample (b) simplified cutting view

Fig. 5.8 Ferrite phase shifter with double magnetic biasing system

Fig. 5.9 shows the experimental setup of the double ferrite slab phase shifter based on the SIW technique. For the calibration, TRL calibration kit described in Fig 3.7 was applied with a test fixture (Wiltron Universal Test Fixture). DC Current was applied to the both ends of the coil using a DC power supplier (Agilent E3610A). While applying DC current to the coil, S-parameters were measured using a VNA (Anritsu 37369D).

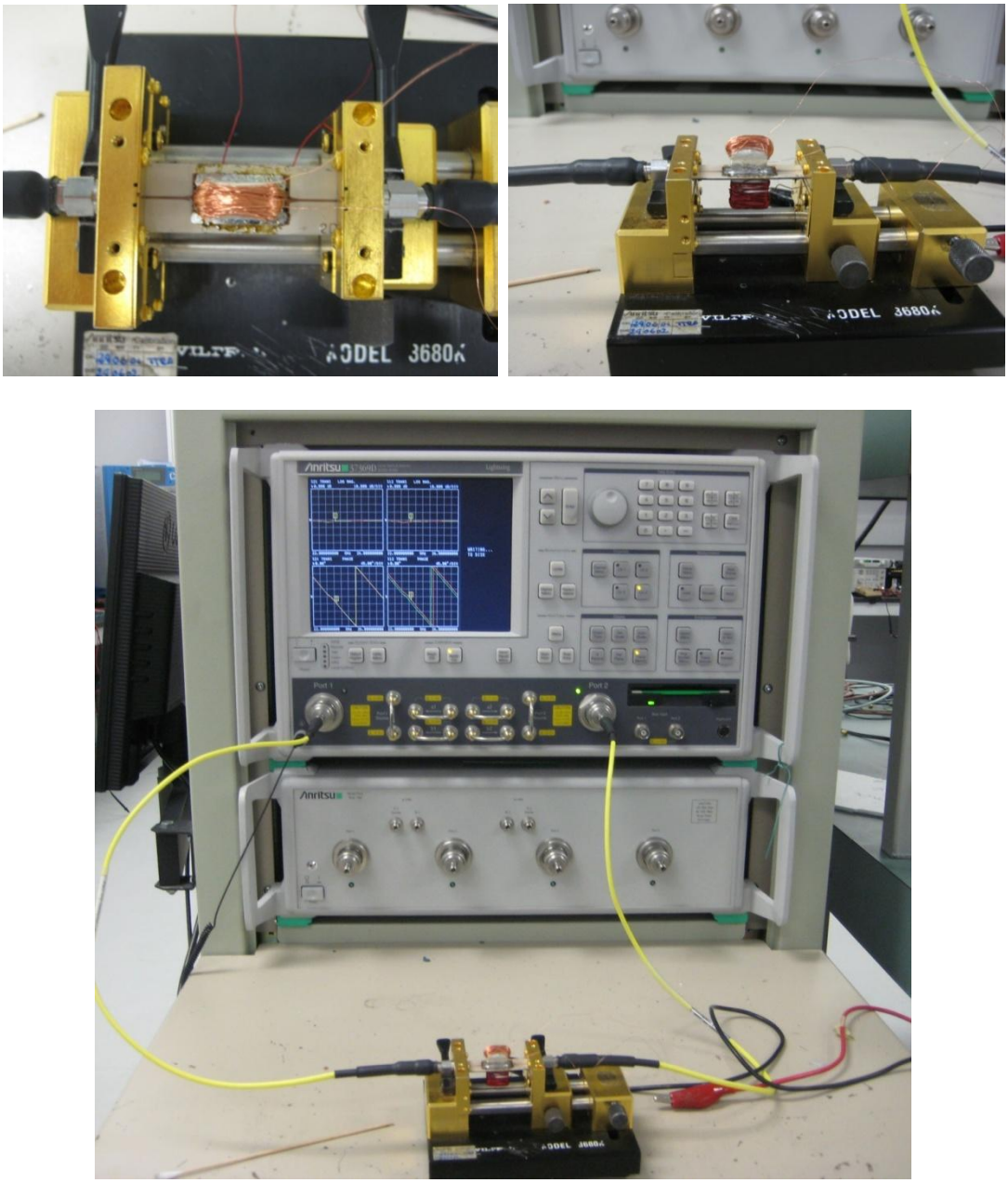

Fig. 5.9 Experimental setup of the double ferrite slab phase shifter

5.3 Results

As a first step of verification, both simulated and measured results of double ferrite slab phase shifter are compared in S-parameter as shown in Fig. 5.10. The simulated result shows that the return loss matching condition is better than 20dB, and the measured result also shows that the matching was better than 18dB for the interested frequency range from 22GHz to 26GHz. As the dielectric constant of the ferrite material is not very far from the dielectric laminate material used in this phase shifter, the matching result of the phase shifter is quite agreeable.

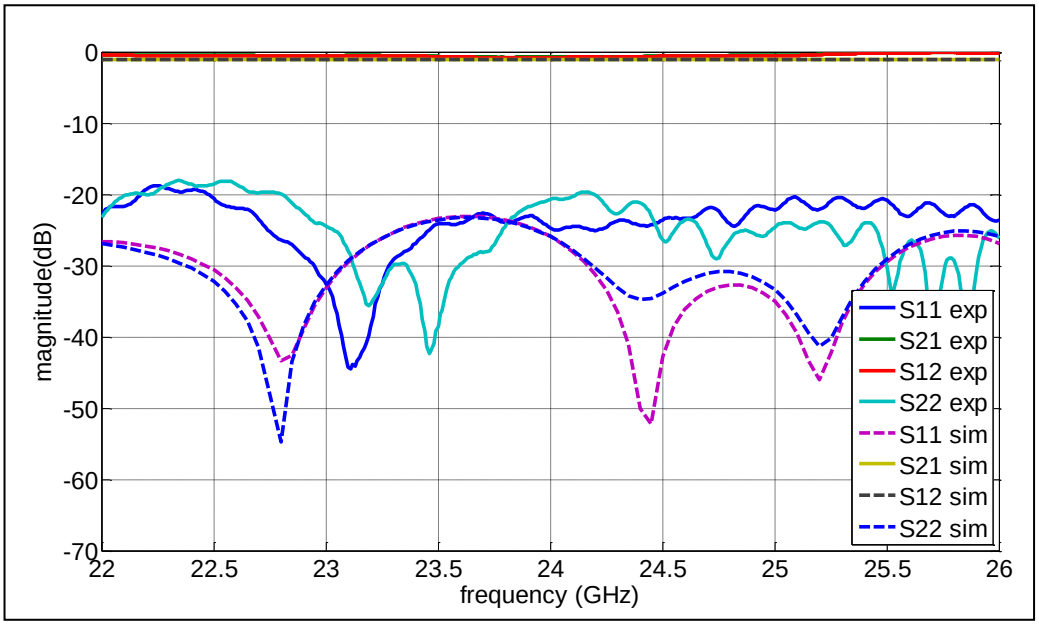

Fig. 5.10 Measured and simulated results of SIW single slab ferrite phase shifter without external magnetic field bias

Fig. 5.11 shows the measured results of phase split between S21 and S12 at 22GHz, 24GHz and 26GHz, respectively by the change of applied current to the coil system. The

applied current is used for *x-axis* to evaluate the phase splitting of the phase shifter instead of magnetic field intensity because there is no proper mean to measure the magnetic field in the given condition.

During our experiments, when the applied current reached to 1A, it generated too much heat on the coil, and the heat started burning the insulation coat on the wire. If it were made possible to use Lithium ferrite for this demonstration, more current could have been applied because only one spike of current would have been required for biasing. But as Nickel ferrite is used instead for the phase shifter, it is necessary to keep holding the applied current to maintain the phase shift value. In this experiment, the maximum current applicable to the phase shifter without a significant heat generation was 1A. It is observed that more phase split is achieved at 22GHz than other higher frequencies as also observed in Fig. 5.4.

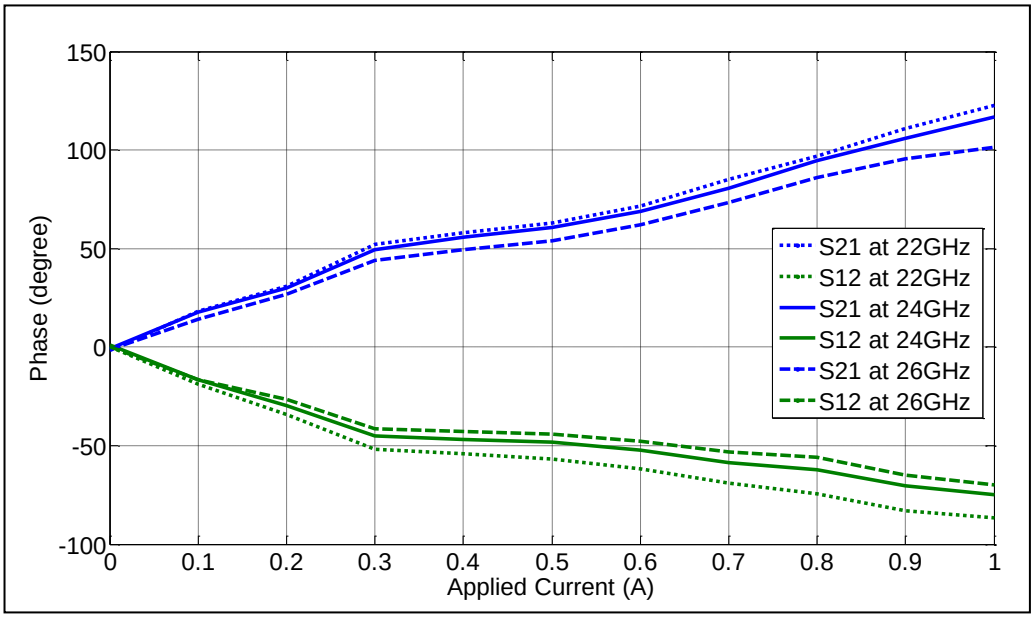

Fig. 5.11 Measured phase split results of double ferrite slab phase shifter

Fig. 5.12 shows the measured phase shifts of the double ferrite slab phase shifter. It is observed that the phase shifter shows a linear increase of phase shift for the increase of the applied current. It means that the phase shifter is operated below saturation magnetization because the effective permeability has a linear decrease up to the saturation magnetization as shown in Fig. 2.6. It is also clearly shown that more phase shift can be achieved at a lower frequency when the saturation magnetization of the ferrite used in the phase shifter is constant.

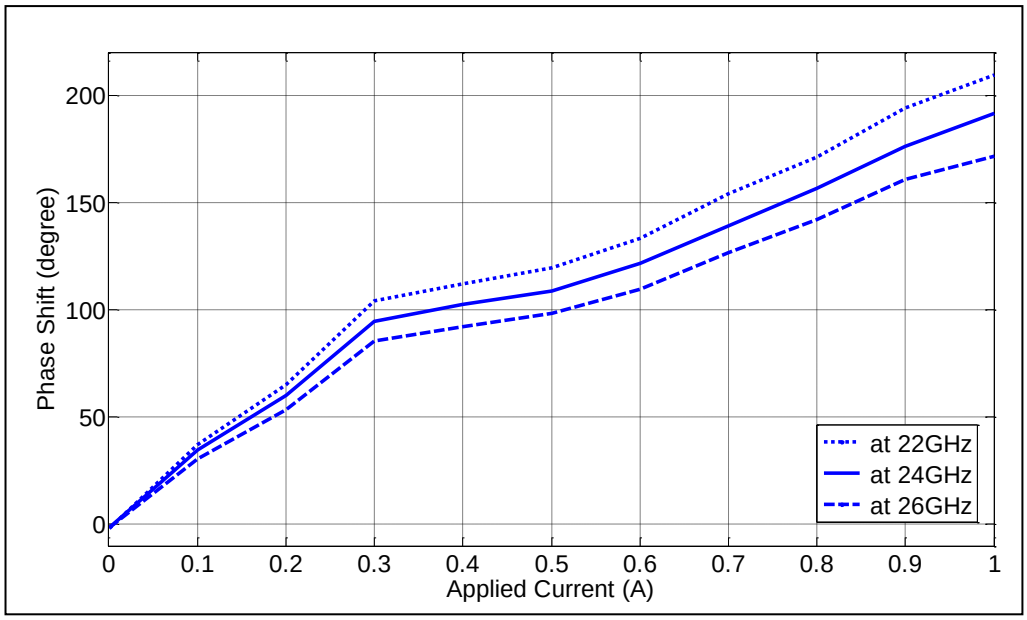

Fig. 5.12 Measured phase shift of double ferrite slab phase shifter

In comparison with the simulated results in Fig. 5.5, it can be assumed that the magnetization achieved through the 1A amount of current was about 3000G. If more current were applied to the phase shifter, about 300° of phase shift at 24GHz may be

achievable as per comparison between Fig. 5.5 and Fig. 5.12. The resulting phase shift achieved in this experiment at 24GHz with 1A applied current is about 190°.

In order to calculate "Figure of Merit" of the double ferrite slab phase shifter using SIW technique, the insertion loss was captured by the change of the applied current. It is observed that the insertion loss of the propagating wave in the forward direction is deviated from that of the wave in the opposite direction when the applied current increases. The difference between S21 and S12 in Fig. 5.13 agrees well with the predicted difference in Fig. 5.6 if the magnetization achieved in measurement is assumed to be about 3000G. And also it is observed that the insertion loss is more dependent on the matching results than the effective permeability variation as there is a significant difference in insertion loss between 22GHz and 26GHz.

The achieved figure of merit at 24GHz with the double ferrite slab phase shifter using SIW technique in this experiment is 95°/dB.

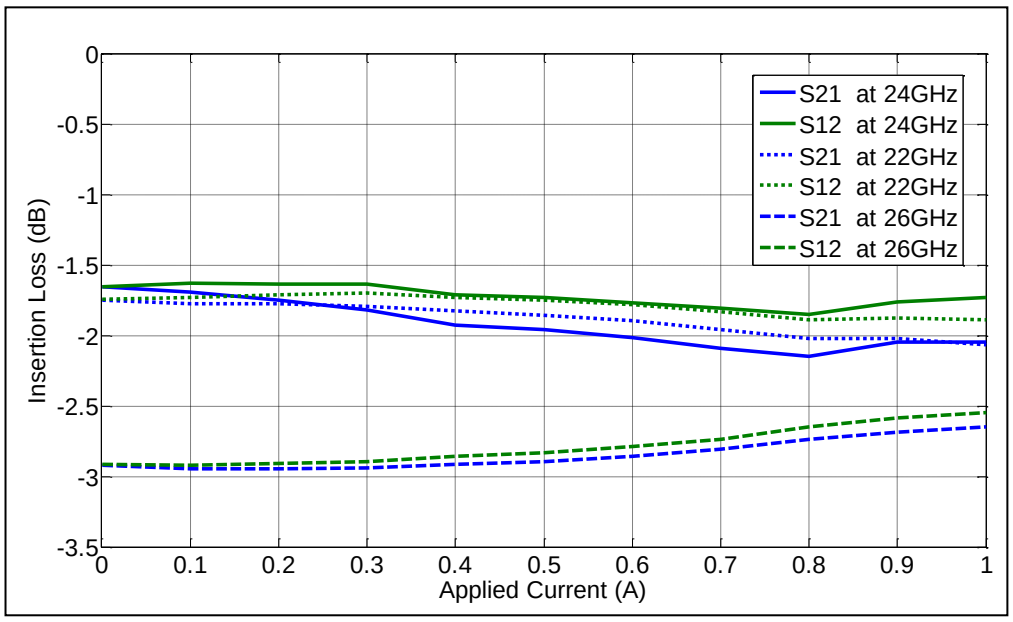

Fig. 5.13 Measured insertion loss of double ferrite slabs phase shifter

5.4 Conclusion

As a practical solution of planar ferrite phase shifters, a simple form of the ferrite phase shifter was devised so that it can be easily fabricated and assembled at low cost as compared with rectangular waveguide devices as well as other planar type of ferrite phase shifters. An integrated static magnetic field bias system was also devised for a practical application. The matching of the ferrite phase shifter over the frequency range from 22GHz to 24GHz was better than 17dB and the insertion losses in various magnetic field bias cases at the same frequency range were better than 3dB. The achieved phase shift at 24GHz with the integrated bias system was about 190° and insertion loss was about 2dB. Therefore, the achieved figure of merit at 24GHz in the

double ferrite slab phase shifter using substrate integrated waveguide technique in this experiment was 95°/dB. Compared with other planar type ferrite phase shifters, this result is promising as we can achieve more ‘Figure of Merit’ in future once we apply more current on the coil by using Lithium ferrite instead of Nickel ferrite.

CONCLUSIONS and FUTURE WORKS

Thesis Summary

Substrate Integrated Waveguide (SIW) is an emerging technique in that we can use the advantages of waveguide in planar form. A contribution of this thesis is that ferrite phase shifters were fabricated in SIW and a good amount of phase shift was achieved with a very simple integration method of the ferrites into SIW.

In order to develop ferrite phase shifters using SIW technique, the ferrite theory was reviewed to understand the effective permeability of inserted ferrites and SIW was studied to design the phase shifter. After reviewing theories, a single ferrite phase shifter was designed, prototyped and characterized using an electromagnet system. Finally, a double ferrite slab phase shifter was designed and experimented with an integrated magnetic field bias system.

Chapter 2 provided the microwave ferrite theory to understand how ferrites behave over microwave frequency range under a biasing magnetic field. As the interested frequency range was selected over K band, the characterization of microwave ferrites was also explained over the same frequency range. Magnetization equation was introduced and tensor permeability was derived. In this chapter, various microwave ferrite materials were compared and described in various methods. Both longitudinally magnetized ferrite and transversely magnetized ferrite at microwave frequencies were described and explained in term of loss, magnetization and effective permeability.

According to various plots presented in this chapter, it was understood that Lithium ferrite and Nickel ferrite were better choices than YIG ferrite for K-band applications.

In Chapter 3, rectangular waveguide theory was briefly discussed at the beginning. Then, it was applied to a planar form of SIW. Based on waveguide theory, specific design rules of SIW for the design of via-hole array and effective width of broad side wall among others were reviewed. For K-band applications, the cut off frequency was deliberately selected to avoid higher-order modes and a simple SIW was modeled and simulated out of Roger 25mil 6010 material using the SIW design rules described in this chapter. For transition from microstrip to SIW, guided-wave impedance of SIW was calculated in order to decide the matched width of mircostrip, then simulations and experiments were followed up to verify the matching condition. As a result of this chapter, an SIW, which has a back to back transition, was designed and compared in both simulation and experiment.

In Chapter 4, a single ferrite slab phase shifter using SIW technique was designed, fabricated and experimented. The optimal location of the ferrite slab in SIW was described and presented in magnetic field simulation. In order to alleviate a mismatching problem between the ferrite slab and the laminate material, a relatively high dielectric constant laminate material was chosen for SIW. Then, it was shown that how a ferrite slab was integrated in a simple form of SIW and how an SIW ferrite phase shifter was completed easily at the ferrite phase shifter devised in this thesis. The matching result of the phase shifter was better than 15dB and the insertion loss was better than 1.5dB. As the ferrite slab has a finite dimension, Shape Demagnetization Factor was introduced

and its value of the ferrite slab was calculated and compared. For magnetization of the ferrite slab in the phase shifter, an electromagnet was used. The internal magnetic field was calculated based on the external magnetic field generated in between the two electromagnet cores and the shape demagnetization factor. To verify the phase shifting, the circular polarizations of the single ferrite slab were visualized using HFSS. The achieved phase shift in both simulation and experiment was more than 150°.

In Chapter 5, a double ferrite slab phase shifter was designed, optimized, fabricated and experimented in the same manner as the single ferrite slab case. One more ferrite slab was added to the single ferrite slab phase shifter on the opposite side of SIW, each ferrite slab had a different direction of biasing magnetic field to be circularly polarized in the same propagating direction. As a practical solution of planar ferrite phase shifters, a simple form of the ferrite phase shifter was devised so that it can be easily fabricated and assembled at low cost as compared with rectangular waveguide devices as well as other planar type of ferrite phase shifters. As a practical ferrite phase shifter, an integrated static magnetic field bias system was devised. For the integration of magnetic field bias system, a closed magnetic field loop was devised and coils were wound around the closed magnetic field loop. As Shape Demagnetization Factor is also an important design consideration for efficient magnetic field biasing, it was designed that the ferrite slab had the same thickness as the gross thickness of the laminate thickness and two broad wall copper claddings of SIW to make sure that there was a minimal non-magnetic air gap in the closed magnetic field loops. Thus, the minimal gap would give a more phase shifting at a given DC current applied to the coils because the internal

magnetic field in the ferrite slabs could be increased. The matching of the ferrite phase shifter over the frequency range from 22GHz to 24GHz was better than 17dB and the insertion losses in various magnetic field bias cases at the same frequency range were better than 3dB. The achieved phase shift at 24GHz with the integrated bias system was about 190° and insertion loss was about 2dB. Therefore, the achieved figure of merit at 24GHz in the double ferrite slab phase shifter using substrate integrated waveguide technique in this experiment was 95°/dB.

Future Work

As a follow-up design of the above ferrite phase shifters, more better matching condition should be studied using numeric calculations and a more refined integration of magnetic field bias system should be devised by the help of a more sophisticated mechanical design.

And as a further research for microwave ferrite devices using SIW techniques, a low cost planar phase array antenna system with integrated ferrite phase shifters can be investigated and developed. On top of this, various ferrite devices can be designed by combining the unique non-reciprocal behaviors of microwave ferrite with the planar SIW techniques so that the microwave ferrite devices can be used for vast commercial applications as well as limited military applications.

REFERENCES

[1] Ince,W.J and Temme D. H.: "Phasers and time delay elements" *Advances in Microwaves*, 1969, 4, *p2-p189.*

[2] Baden-Fuller, A.J. "Ferrites at microwave frequencies", *Peter Peregrinus Ltd*,1987.

[3] Wenquan Chel, EdwardKai-Ning Ytmngl and Kr Wu, "Millimeter-wave Substrate Integrated Waveguide Ferrite Phase Shifter For Wireless Communicatin Application", *2003 IEEE Topical Conference on Wireless Conimunication Technology*.

[4] Joey R. Bray, Member, IEEE, and Langis Roy, "Development of a Millimeter-Wave Ferrite-Filled Antisymmetrically Biased Rectangular Waveguide Phase Shifter Embedded in Low-Temperature Cofired Ceramic", *IEEE Transactions On Microwave Theory And Techniques*, Vol. 52, No. 7, July 2004.

[5] William D'Orazio and Ke Wu, "Substrate-Integrated-Waveguide Circulators", *IEEE Transactions On Microwave Theory And Techniques*, Vol. 54, No. 10, October 2006.

[6] Wert, C.A., R.M. Thomson, "Physics of Solids", *New York: McGrow-Hill*, 1970.

[7] Baden-Fuller, A.J. "Ferrites at microwave *frequencies*", *Peter Peregrinus Ltd*,1987. *p17~p21*

[8] Symon, K.R., "Mechanics*"*, Reading, *MA: Addison-Wesley*, 1971.

[9] Landau, L and Lifshitz, E., "On the theory of dispersion of magnetic permeability in ferromagnetic bodies", *Physik Z. Sowjetunion, 1935, 8, p. 153-p169.*

[10] Baden-Fuller, A.J. "Ferrites at microwave frequencies", *Peter Peregrinus Ltd,*1987. *P22-P25.*

[11] Polder, D., "On the theory of ferromagnetic resonance" *Phil. Mag., 1949, 40*, pp 99-115.

[12] D. Deslandes and K.Wu, "Integrated microstrip and rectangular waveguide in planar form" *IEEE Microw. Wireless Compon. Lett.*, vol. 11, no. 2, pp. 68–70, Feb. 2001.

[13] David M. Pozar, 'Microwave Engineering', *Wiley*, 1998 Chapter 3.

[14] David M. Pozar, 'Microwave Engineering', *Wiley*, 1998 pp129.

[15] K. Chang, I. Bahl and V. Nair RF, "microwave circuit and component design for wireless systems", *John & Sons*, 2002.

[16] Il-Woo Lee, "Spurious suppressed SIW Filter using stepped impedance resonator structure", *Ajou University, 2007*

[17] J. Xiaoma, "Substrate Integrated Waveguide E-Plane Coupling Dual-Mode Cavity Filter Synthesized With Arrays Of Metallic Via Slots", *Ecole Polytechique Montreal*, 2006.

[18] Feng. Xu, and Ke Wu, "Guided-Wave and Leakage Characteristics of Substrate Integrated Waveguide" *IEEE Trans. on MTT., Vol. MTT-53, No.1, pp.66-73,* Jan. 2005.

[19] Clarricoats, P.J.B., "Microwave Ferrite", *New York, John Wiley and Sons*, 1961.

[20] D. K. Linkhart, "Microwave Circulator Design", *Artech House*, 1989.*p117-p121*

[21] David M. Pozar, "Microwave Engineering, *Wiley*, 1998, *p.518*

[22] David M. Pozar, "Microwave Engineering" *Wiley*, 1998, *p.520*.

[23] David M. Pozar, "Microwave Engineering" *Wiley*, 1998, *p.521*

[24] D.X. Chen et al, "Transverse demagnetizing factors of long rectangular bars: I. Analytical expressions for extreme values of susceptibility", *Journal of Applied physics*, volume 91, number 8

[25] David M. Pozar, "Microwave Engineering" *Wiley*, 1998. *p.522*

[26] David M. Pozar, "Microwave Engineering" *Wiley*, 1998. *p.522*